ARMY RESEARCH LABORATORY

An Electroacoustic Hearing Protector Simulator That Accurately Predicts Pressure Levels in the Ear Based on Standard Performance Metrics

by Joel T. Kalb

ARL-TR-6562 **August 2013**

RDRL-HRS-D 3 September 2014

MEMORANDUM FOR SEE DISTRIBUTION

SUBJECT: ARL-TR-6562, "An Electroacoustic Hearing Protector Simulator That Accurately Predicts Pressure Levels in the Ear Based on Standard Performance Metrics," August 2013, by Joel T Kalb

Change: Figure captions 1, 3, and 5 have been revised in the published report.

Reason: Permission statements were added to the captions. Please discard the previous version of this report.

Joel T. Kalb

Encl:

Joel T Kalb
Perceptual Sciences Branch

NOTICES

Disclaimers

The findings in this report are not to be construed as an official Department of the Army position unless so designated by other authorized documents.

Citation of manufacturer's or trade names does not constitute an official endorsement or approval of the use thereof.

Destroy this report when it is no longer needed. Do not return it to the originator.

Army Research Laboratory
Aberdeen Proving Ground, MD 21005-5425

ARL-TR-6562 **August 2013**

An Electroacoustic Hearing Protector Simulator That Accurately Predicts Pressure Levels in the Ear Based on Standard Performance Metrics

Joel T. Kalb
Human Research and Engineering Directorate, ARL

REPORT DOCUMENTATION PAGE	Form Approved OMB No. 0704-0188

1. REPORT DATE *(DD-MM-YYYY)*	2. REPORT TYPE	3. DATES COVERED (From - To)
August 2013	Final	January 2010–January 2013

4. TITLE AND SUBTITLE
An Electroacoustic Hearing Protector Simulator That Accurately Predicts Pressure Levels in the Ear Based on Standard Performance Metrics

5a. CONTRACT NUMBER

5b. GRANT NUMBER

5c. PROGRAM ELEMENT NUMBER

6. AUTHOR(S)
Joel T. Kalb

5d. PROJECT NUMBER
0601102A 74A

5e. TASK NUMBER

5f. WORK UNIT NUMBER

7. PERFORMING ORGANIZATION NAME(S) AND ADDRESS(ES)
U.S. Army Research Laboratory
ATTN: RDRL-HRS-D
Aberdeen Proving Ground, MD 21005-5425

8. PERFORMING ORGANIZATION REPORT NUMBER
ARL-TR-6562

9. SPONSORING/MONITORING AGENCY NAME(S) AND ADDRESS(ES)

10. SPONSOR/MONITOR'S ACRONYM(S)

11. SPONSOR/MONITOR'S REPORT NUMBER(S)

12. DISTRIBUTION/AVAILABILITY STATEMENT
Approved for public release; distribution is unlimited.

13. SUPPLEMENTARY NOTES

14. ABSTRACT

Impulse-noise response pressure waveforms in the occluded volume under a hearing protector (HP) depend on energy transmission by means of its rigid motion, through its material and at skin-contact leaks. The Real Ear Attenuation at Threshold (REAT) and Microphone in Real Ears (MIRE) methods are common insertion loss measures of this process at a collection of low-level test frequencies. This paper describes a linear HP simulation with an electroacoustic (EA) simulator determined with an iterative fitting procedure using the insertion loss data. Combining this simulator with head diffraction and ear-canal models in the Auditory Hazard Analysis Algorithm for Humans (AHAAH) allows free-field pressure waveforms to be transformed to protected waveforms measured at various locations in real and artificial ears by solving the differential equations of motion. Applying the EA simulator to 384 REAT data-sets from an inter-laboratory study using ANSI S12.6 method B for inexperienced subject self-fits gives statistical frequency distributions of occluded volume, leakage elements, and predicted hazard with the four tested HPs and a rifle waveform. Further validation was obtained using manufacturer-supplied REAT data to predict and compare with protected waveforms on humans and manikins near impulse noise sources such as high-explosives, rifles, shoulder-fired recoilless rifles, and howitzers.

15. SUBJECT TERMS
hearing protector, simulator, impulse, noise, hazard, model

16. SECURITY CLASSIFICATION OF:			17. LIMITATION OF ABSTRACT	18. NUMBER OF PAGES	19a. NAME OF RESPONSIBLE PERSON
a. REPORT	b. ABSTRACT	c. THIS PAGE			Joel T. Kalb
Unclassified	Unclassified	Unclassified	UU	56	19b. TELEPHONE NUMBER (*Include area code*) 410-278-5977

Standard Form 298 (Rev. 8/98)
Prescribed by ANSI Std. Z39.18

Contents

List of Figures

List of Tables

1. Introduction

1.1 Background and Motivation

Soldiers operate in noisy environments. The noises they encounter include continuous noise, such as from generators or vehicles, and impulse noises, such as from explosions or gunfire. Although some of these noise hazards (e.g., enemy gunfire) are outside the U.S. Army's control, many other noises are generated by our own equipment. To protect our Soldiers' hearing, it is imperative we understand how hazardous these noise exposures are and, by extension, how materiel developers and risk managers can control and mitigate the hazards.

Understanding of the dynamics of hearing hazard from continuous noise exposure is a mature field. As a result, national and international standards exist regarding exposure and the use of hearing protection devices (HPDs), including earplugs and earmuffs, to protect hearing. However, impulse noise exposure is not as well-documented as other noise hazards. Impulse noise peak pressure levels are much higher (150 dB for pistols to 190 dB for howitzers and mortars) and durations are much shorter (0.5 ms for pistols to several milliseconds for howitzers) compared to the high-level continuous noise (110 dBA in tanks to 140 dBA near aircraft). The restrictions on impulse noise exposure, typically presented for weapons firing as allowable number of rounds (ANOR) per day, have historically erred on the conservative side (MIL-STD-1474 D, 1997). This has led to unnecessary restrictions on the ANOR and, in some cases, not allowing any rounds at all to be fired from available or proposed weapons. Such approach may cost Soldiers' lives since it does not allow the Soldiers to use all available means to deter enemy's force.

To protect Soldiers' hearing and permit them to use high but physiologically safe firepower, a physiologically based model of hearing hazard—Auditory Hazard Analysis Algorithm for Humans (AHAAH)—has been developed by the U.S. Army Research Laboratory (Price, 2007). AHAAH takes as input the waveform of an impulse noise and outputs the hazard associated with it, expressed as Auditory Risk Units (ARUs).

One limitation of the AHAAH model is that it assumes that the waveform is either acting on an unprotected ear or, if the user chooses, assumes the presence of a generic hearing protector. This solution is frequently insufficient since it does not allow developers to determine and assess appropriate hearing protection required to mitigate the hazard. Soldiers protect their hearing by wearing hearing protection in almost all operational scenarios, and it is highly desirable to extend AHAAH with a flexible hearing protector simulator (HPS) that can account for the effects of various HPDs to impulse sound exposure without the need for costly, time-consuming, and repetitive field tests. Such a physics-based mathematical simulator can modify free-field (FF) waveforms entering the AHAAH model to reflect the effect of the particular HPD on sound waves impinging on the Soldier's ear. The modified waveform can then be used as input to the AHAAH

model to calculate accurate noise hazards affecting the Soldier. This report describes the basics of the HPS developed to account for any linear HPD and to be a front-end simulator for the AHAAH model. (Although this HPD simulator has been specifically developed to use with the AHAAH model, it can serve as a stand-alone HPS as well.)

1.2 Basics of the Hearing Protector Simulator

The proposed HPS models a hearing protector in terms of the electrical analogs of the HPD's acoustical elements. Three pathways of the HPD are modeled: the effect of the mass of the HPD, the leakage of acoustic energy around the device, and the material transmission of the energy through the device. All three paths are modeled as pistons, each having the basic parameters of low-frequency loss, α (dB), the resonant frequency, f (kHz), and the dimensionless quality factor, Q. The outputs of all three pathways then interact with the occluded volume (OV) of the HPD (the volume of air between the HPD and the tympanic membrane [eardrum]).

The development of the parameters associated with each specific HPD is based on physical or perceptual measures of the attenuation of the HPD. Physical measures include the use of acoustic test fixtures (ATFs) to measure attenuation of noise or the use of the microphone-in-real-ear (MIRE) method using humans (ANSI 12.42, 2010). MIRE and ATF recordings can be performed using pure tones or narrowband noises for the frequencies of interest, or by using a broadband stimulus that can be analyzed with Fourier transforms to yield frequency information. The perceptual measure used is the real-ear-attenuation-at-threshold (REAT) method (ANSI 12.6, 2008). REAT is performed at threshold-of-hearing levels using narrowband noise centered on the seven audiometric frequencies of 125, 250, 500, 1000, 2000, 4000, and 8000 Hz. Any of these measures are acceptable for development of parameter estimates.

REATs can only be accomplished with continuous noise sources; ATFs can be used for either continuous or impulse noise attenuation measures. Generally, MIRE is not used for impulse measures, as the wire leading to the microphone in the ear canal of the listener can break the seal of the HPD and degrade its performance, leading to increased exposure to the wearer. Also, humans cannot be subjected to a large number of impulse sounds in this type of measurement environment due to ethical and legal restrictions. Moreover, it is assumed that the HPDs act in a linear way—that is, the amount of attenuation provided does not vary depending on the impulse noise level.

There are two main types of attenuation measured: noise reduction (NR) and insertion loss (IL). NR is a measure of the difference between the FF noise level and the level at the eardrum of the listener. IL is the difference between the level at the eardrum with and without the HPD. Because the ear naturally amplifies sound, IL is always equal to or greater than NR.

The intention of the HPS was to extend the AHAAH model application to all types of worn hearing protection to provide a realistic estimate of noise hazard for any listening situation involving impulse noise. The simulator will also allow us to improve weapon and HPD designs by predicting protected responses to FF waveforms using commonly available REAT HPD data.

Because it depends on the HPD mechanics and support at the ear, the simulator applies to any future HPD design and to variability in the way the HPD is worn.

1.3 Background of Physical Electroacoustic Modeling

1.3.1 Standard and Improved HPS

Studies of sound transmission through the unprotected or protected ear traditionally start with analysis of energy flow through schematic diagrams based on electroacoustic (EA) analogies between acoustical elements and their electrical counterparts. These elements are identified by anatomical and physical structures, as shown in figure 1 (Schröter, 1983; Schröter and Pösselt, 1986; Shaw and Thiessen, 1958, 1962; Zwislocki, 1957). The analysis method tracks energy flow through fluid and solid pathways and can include electrical component transducers, such as microphones and loudspeakers. The equations of sound energy transmission in acoustic devices are the same as the equations for voltage changes in the electrical networks; the elements of both types of circuits are shown in figure 2 (Beranek, 1954; Kinsler and Frey, 1962). Some elements may not be constant, depending on their displacement, velocity, or temperature. These influences can be included in the circuit differential equations and solved by numerical integration to give pressure under the HPD. Assuming these elements are fixed at low stimulus levels, these equations can be transformed by Fourier analysis into rational complex polynomials that can be solved and compared to measured transfer function magnitudes and phases between various parts of the HPD or ear. The constants in the linear solution serve as starting values for the time domain calculations and nonlinear models at higher-level excitation.

The HPS described in this report applies to both earmuff-type and earplug-type HPDs and is a three-piston model with individual pistons controlling HPD behavior in the low-, medium-, and high-frequency range, respectively.

The central component of the simulator is a main piston (MP) formed by the HPD mass supported by the compliance and damping of the skin contact. It represents the middle transmission path in the right side of figure 1. This idealized MP is rigid, leak-free, and moves under pressure from the external sound to compress the OV behind the piston with resulting sound pressure at the eardrum. Appendix A analyzes a single piston in the time and frequency domains, giving transfer function solutions and plots showing key features of the frequency response functions. These functions include the low-frequency attenuation, α_1 (dB), the resonant frequency, f_1 (kHz), and a dimensionless quality factor, Q_1. These values can be identified by inspecting REAT data and can be related to the acoustical parameters shown in figure 1. This path dominates energy transmission for well-fitted plugs and muffs below f_1, which is typically 1 to 2 kHz. Values for α_1 range from –20 to –30 dB and depend on the stiffness of the skin-cushion support relative to the acoustic compliance of the OV. The Q_1 factor can vary from 0.5 for a high-damping piston to 2.5 for a low-damping piston.

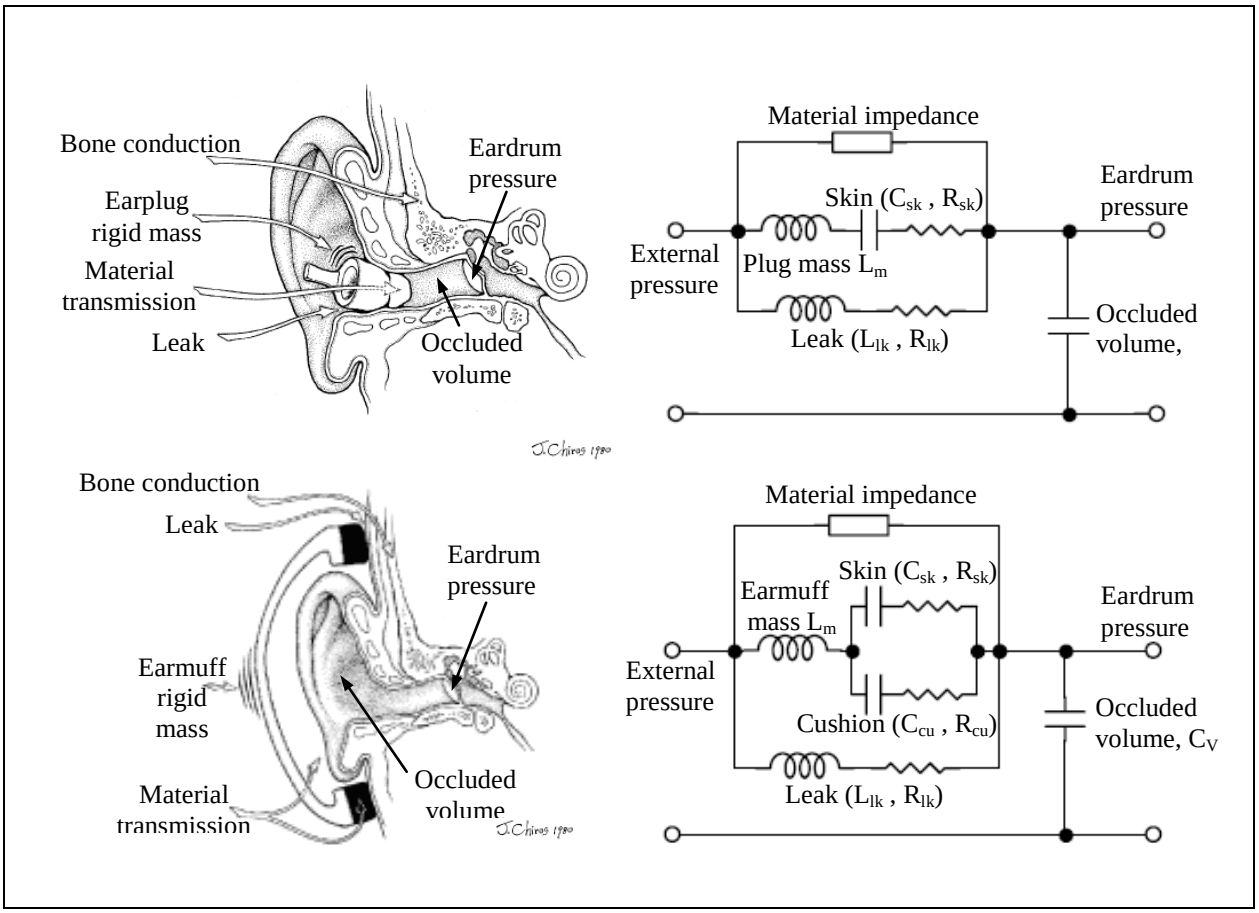

Figure 1. Acoustical and electrical diagrams of earplug and earmuff showing HPD simulator elements for energy flow paths. (Ear graphic adapted from, and courtesy of, E. H. Berger, 3M Personal Safety Division, St. Paul, MN.)

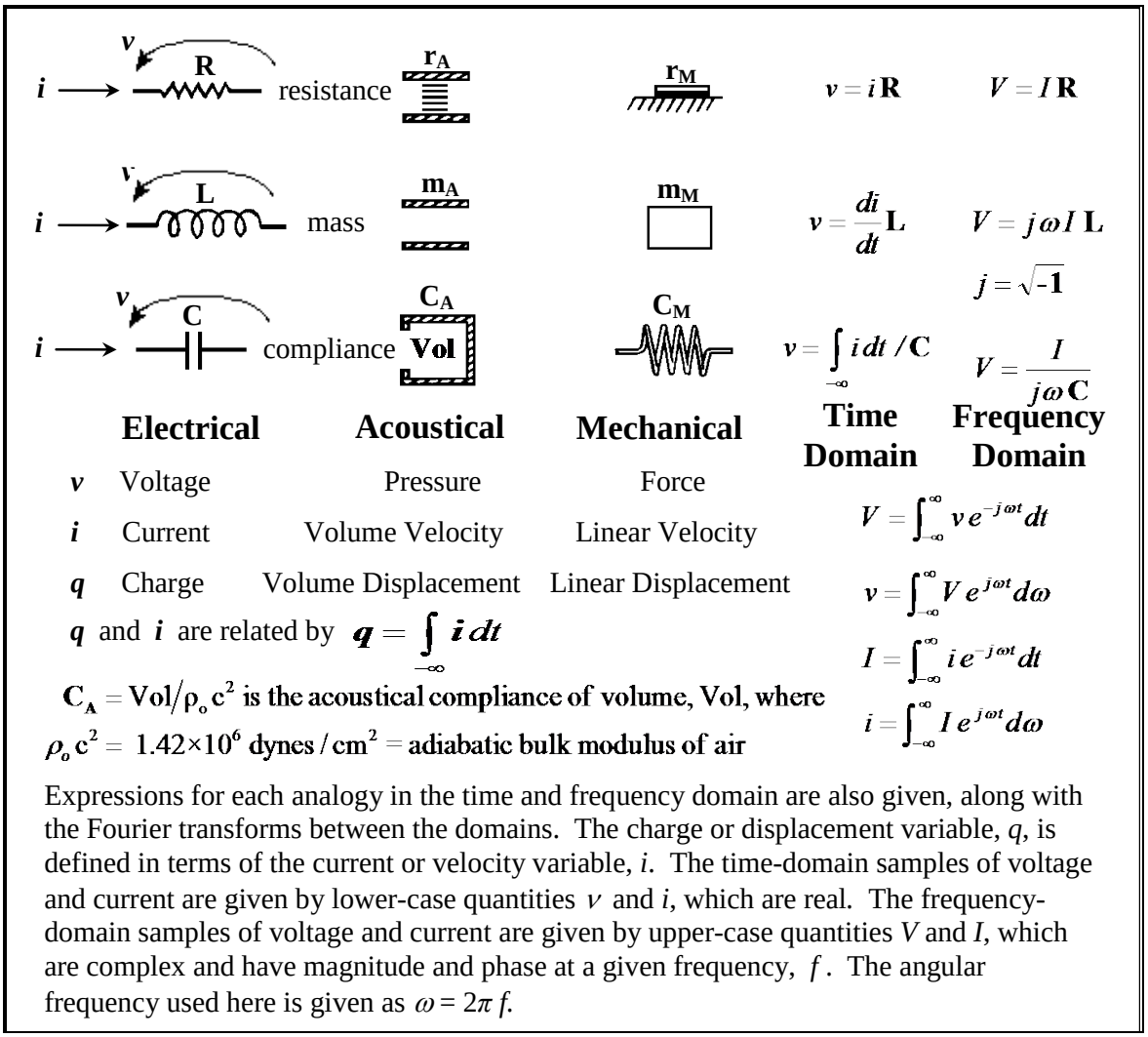

Figure 2. List of AE analogies showing basic components of resistance, mass, and compliance in electrical, acoustical, and mechanical form.

As shown in figure 1, the leakage piston (LP) path bypasses the MP. For moderate-leakage HPDs, the low-frequency loss, α_2 , approaches 0 dB, and there is often a low Q (less than 1.5) resonance at f_2 less than 63 Hz. This path is also modeled as a piston where the mass is a plug of air particles moving in phase. The resistance is due to the viscosity of moving air at the surfaces surrounding the leak path. This piston represents the lowest transmission path shown in the right panel of figure 1. There is no support compliance since the air is not blocked. The leak values are given (Beranek, 1954) in terms of the area and length of the leak path. Values for f_2 can extend up to 2 kHz for large leaks, and the quality factor, Q_2, is generally low at 0.5 since damping is high. Occasionally Q_2 is higher at values of 3 when the mass and resistance form a Helmholtz resonator by acting together with the OV compliance.

Above the MP resonant frequency the transmission falls at 12 dB per octave, assuming a rigid piston mass without multimodal vibrations in the piston structure at higher frequencies (Shaw and Thiessen, 1962). Sound transmission through this material path was included as a third element by Zwislocki and Schröter, but they gave no further details. This transmission path is shown as the top path in the right side of figure 1. Here it is assumed that the vibrations can be lumped into a secondary piston (SP) mounted within the otherwise rigid MP and having a higher resonant frequency, f_3, between 4 and 8 kHz. Material damping varies considerably giving a quality factor, Q_3 ranging from 0.2 to 10. This material path is thus another rigid piston with a mass supported by its own compliance and resistance within the MP. Since the SP can be stiffly supported within the MP, values of the low-frequency loss, α_3, which depend on the ratio of this stiffness to that of the OV, can be between –20 and –40 dB. This model ignores energy flow paths through bone conduction and through the earmuff cushion, as shown in figure 1, as having a negligible effect compared to the other three paths.

The EA method combines acoustical elements, such as ducts and OV cavities, with mechanical elements, such as HPD mass and cushion seal viscoelasticity. Assuming that the sound wave impinges on a cross-sectional area A of the HPD, the mechanical mass and resistance can be converted to acoustical mass and resistance by dividing them by A^2, and the acoustical compliance will be equal to the mechanical compliance multiplied by A^2. For simplified notation, each compliance C is written as a respective stiffness, K, which is the reciprocal of compliance.

1.3.2 Standard Characterization of Hearing Protection Performance

Reduced sound transmission through a hearing protector can be expressed by either IL or NR and measured using MIRE or ATFs. The concepts of IL and NR are shown in figure 3 where the *A* and *B* terms are sound pressure levels in decibels, and the prime denotes values obtained with the HPD in place. Test stimuli can be sinusoid (MIRE, ATF), narrowband noise (REAT), broadband noise (MIRE, ATF), or an impulse waveform (ATF). In the last case, a one-third octave band analysis gives equivalent levels taken over a time interval larger than the blast duration. Losses and gains are expressed as negative and positive numbers, respectively.

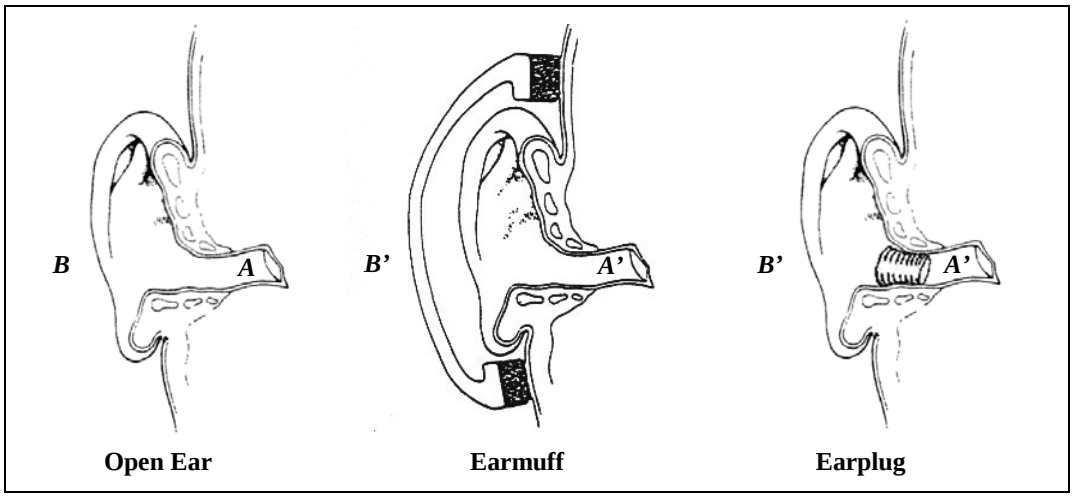

Figure 3. Ear diagrams showing measurements with differing hearing protection. (Ear graphic adapted from, and courtesy of, E. H. Berger, 3M Personal Safety Division, St. Paul, MN.)

The outside location should be close to the head or hearing protectors without FF disturbance so that $B' \approx B$. Three functions can now be defined in terms of these measurements:

$A' - B' \equiv$ NR

$A' - A \equiv$ IL

$A - B \equiv$ transfer function of the open ear (TFOE) or head-related transfer function.

For humans, the IL is the difference between thresholds of hearing (REAT) or the difference in microphone recordings (MIRE) (Berger, 1986). All quantities are functions of propagation angle, θ, with the worst case assumed to be normal incidence $\theta = 90°$ (sound propagates perpendicular to the temporal side of the head and into the ear canal). Other cases are grazing incidence where $\theta = 0°$ when the listener faces the source, full head shadow where $\theta = 270°$, and random incidence where θ is averaged over all angles. The levels measured in the ear must be measured at the same location, which is assumed to be at the eardrum. The IL calculation requires two sound pressure measurements for which the FF stimulus is assumed to be the same, while the NR is more conveniently measured both outside and under the HPD for the same stimulus. For small-arms sources, the shot-to-shot variability is negligible because of the close tolerances of propellant and mechanical construction of the cartridge, and lack of fluctuations due to secondary detonations outside the gun barrel. Weapon blasts often cannot be used to measure the IL with either human or manikin ears because in the open ear condition, the level at A would be hazardous or might overload the manikin microphone. Perceptually derived REAT magnitudes at low listening levels are generally the same as objectively derived MIRE magnitudes at higher sound levels except at frequencies below 63 Hz where subjects hear physiological noise in addition to the stimulus (Berger, 1986). TFOEs have been tabulated for numerous incident angles for both humans and manikins (Mehrgardt and Mellert, 1977; Shaw and Vaillancourt, 1985) and are assumed level independent.

The following discussion shows how these functions incorporate hearing protection into the AHAAH unprotected ear model, which applies to the open ear case. Here the FF wave, *B* encountering the head is diffracted and reflected before it enters the concha, reflects in the ear canal (Wiener and Ross, 1946) and becomes the eardrum wave, *A*. This process is described by EA elements in the AHAAH model in order to calculate the response waveforms and TFOE functions at either the entrance or eardrum termination of the ear canal (Price and Kalb, 1991). Figure 4 shows good agreement for the TFOE at normal incidence for humans in Shaw and Vaillancourt in red, Mehrgardt and Mellert in blue, the French-German Research Institute of Saint Louis (ISL) ATF in black (Parmentier et al., 2000), and the AHAAH model in green.

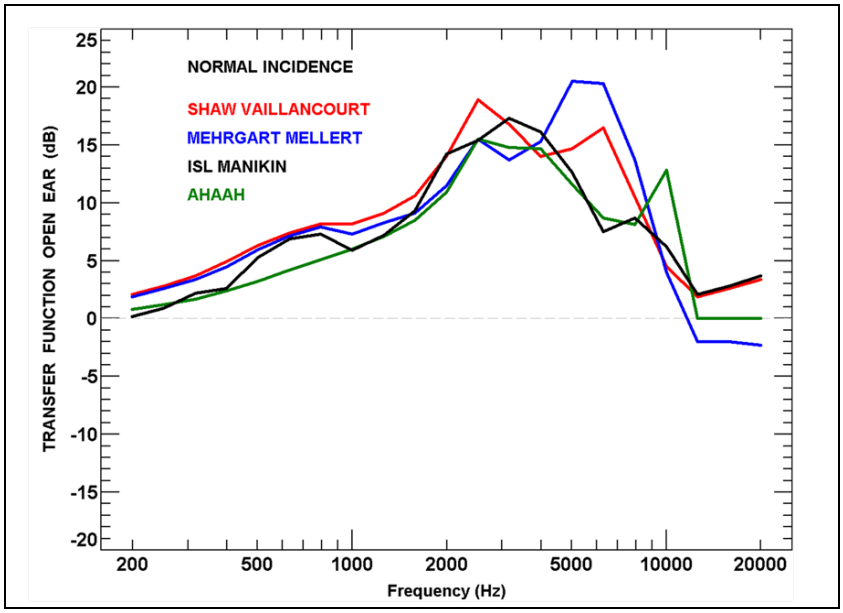

Figure 4. Normal incidence TFOE measurements for humans.

Just as the TFOE and associated AHAAH elements describe the properties of the open ear without the HPD, the IL function and associated HPD circuit elements describe the properties of the HPD independently from the head.

While it is evident that the earmuff and earplug strongly influence the sound field in the space in front of and behind the protectors, these disturbances are reduced farther away on the head and near the eardrum, leaving the EA elements in those regions unaltered. Because the IL involves the difference between the open ear and protected ear transmission, fixed factor effects, such as head reflection, diffraction, transmission in parts of the ear canal unoccupied by the HPD, and eardrum reflections, will cancel. Other factors will change between the two IL measurements, such as near-protector sound fields, material support details, and leaks at the protector-skin interface and transmission in parts of the ear canal occupied by the HPD. They influence the sound measurement *A'* and therefore are accounted for in the IL function as being solely due to the HPD. Likewise, these same factors determine the HPD simulator, making it a suitable description of the IL function.

Based on the transfer function definitions, these quantities are related by the expression NR = IL + TFOE. This means that the NR, which depends on both the head and HPD, can be separated into two parts: the IL part depending on the HPD and the TFOE part depending on the head. Assuming this formula applies for all frequencies and phases, we are able to calculate the waveform under a hearing protector, resulting from an FF waveform—namely, a noise reduction calculation. First, the IL simulator is applied to the FF pressure waveform, giving a preattenuated FF waveform. Next, the preattenuated waveform is applied to a now opened ear using the AHAAH model to transfer it to either the eardrum or canal entrance location. This waveform can then be compared to measurements on either human or manikin ears to test the validity of the fitting and transfer process. Finally, this waveform can be further propagated into the AHAAH model for hazard assessment (appendix B).

1.4 Interlab Study: REAT Data

The Interlab study (Royster et al.,1996) in which users self-fit hearing protectors (ANSI S12.6-2008 method B: user fit) with no experimenter instruction gives an estimate of the variability expected in collecting REAT data. Four laboratories each tested 24 subjects with four repetitions totaling 384 sets of data. The hearing protectors were three earplugs (E.A.R. foam, Willson EP100 double-flange, and V-51R single-flange) and one earmuff (Bilsom UF-1) (figure 5). Figure 6 shows plots of the 384 sets of REAT values for each of the four hearing protectors. The figure shows large variability of data as expected from the naive user-fit procedure due to their choice of size, depth of insertion, and misalignment. Each variable is a source of fitting error and results in different frequency distributions in the REAT values. The largest range occurred for the multiple-sized V-51R and EP100 plugs, while the lowest variability was for the earmuff. The E.A.R. foam earplug can be inserted into the ear with various depths, which is known to cause some variability; this variability is reflected in the study results.

Because mean REAT values are poor indicators of achieved HPD performance, an adjustment factor to account for the expected variability of the data is frequently applied in practical applications. Many schemes exist for estimating the appropriate adjustment, but it is common practice to reduce the performance by 1 standard deviation. Better estimates are possible when the influence of fit is better understood. In the current HPS development, an individual model is fitted to each data set, giving 384 sets of values for the suspension, leakage, and OV. Distributions of these quantities show the underlying variability of the user fit. Using each model fit and a given impulse waveform, a distribution of hazard is expected because the fitting errors can be demonstrated.

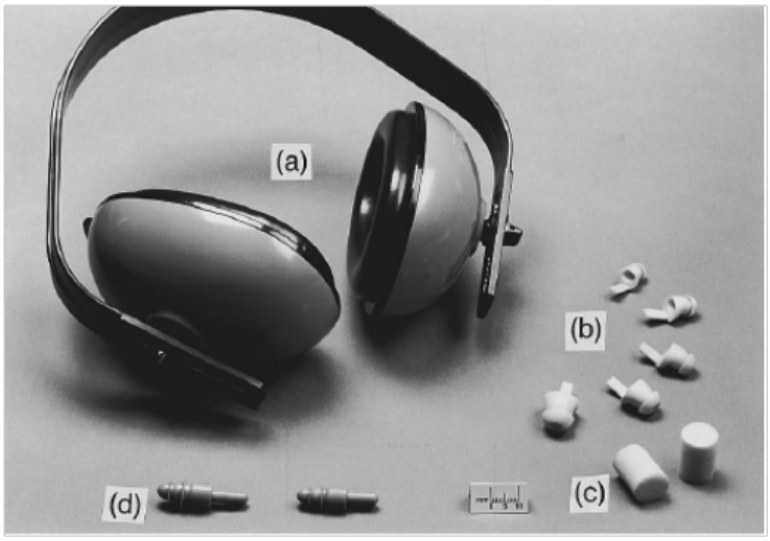

Figure 5. Four hearing protectors used in the Interlab study. (a) Single size Bilsom UF-1 earmuff worn in the standard band-over-the-head configuration, (b) V-51R premolded single-flange earplug in five sizes, (c) E.A.R. single size disposable foam earplug, and (d) Willson EP100 premolded double-flange earplug in two sizes. The scale shown is 1 cm. (Reproduced with permission from Royster et al. Development of a New Standard Laboratory Protocol for Estimating the Field Attenuation of Hearing Protection Devices. Part I: Research of Working Group 11, Accredited Standards Committee S12, Noise. *Journal of the Acoustical Society of America* 1996, *99*, 1506–1526. Copyright 1996, Acoustical Society of America. http://dx.doi.org/10.1121/1.414729)

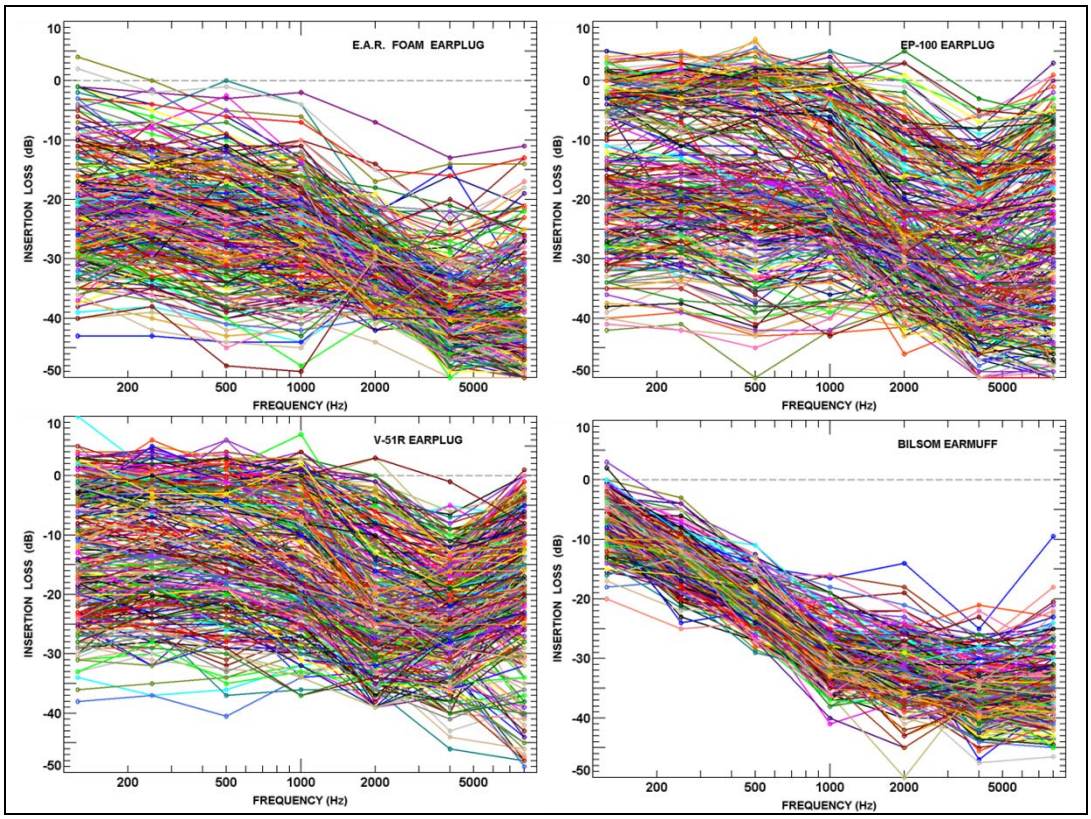

Figure 6. REAT data for four hearing protectors determined by four laboratories in the Interlab study.

2. Analysis

The task of finding a set of circuit elements for the three piston paths and OV shown in figure 1 is complicated because in conducted calculations (see appendix A), the number of unknown quantities (9 for the earplug or 11 for the earmuff) is larger than the number of known quantities (typically 7 IL data points). These equations are nonlinear functions of frequency and are complex, meaning that interference occurs because of phase differences between the energy flow in each path of the model. This difficulty is overcome by the assumption that each path has a simple piston response and a resonant frequency that is low for the LP path, medium for the MP path, and high for the SP path, and the resonant frequencies do not overlap. A sequential fitting procedure using this assumption is described in appendix C.

The procedure involves taking circuit elements in each path one at a time and incrementally adjusting them over a given percentage range, while the other two paths are fixed, and then summing the squared errors over the associated subset of the IL data points to find improved circuit element parameter values. This process is repeated so that all circuit values are varied by percentage increments of 0.1%, 1%, and 10% of the current value at each step. The range of values covers 10 increments below the previous value to 10 increments above it. To prevent divergence of the circuit elements due to interactions between each flow path, the frequency domain description values for each path are calculated (α, f, Q) and compared with preassigned limits. Any value exceeding these limits is replaced by the range limit, and the circuit elements are recalculated from the frequency domain values according to the results in appendix A. Eventually, after a number of calculation cycles, the IL results are plotted along with IL data for the individual and combined paths. Good agreement shows that simultaneous fits of circuit elements in each of the three paths have been achieved. As a further accuracy test, the acoustic circuit elements can be transformed into mechanical mass, stiffness, and resistance; these values are then compared with known mechanical values.

3. Results and Discussion

Eight selections from the 384 REAT model fits for each protector of the Interlab study are shown in figures 7–14. Pressure transfer function magnitudes for individual and combined model path transmission are plotted for comparison with REAT data (triangles). The contribution of the MP rigid piston path is gray, the LP leakage path is blue, the SP material deformation path is black, and the combination of all three is green. The combined path model green line and the REAT data closely agree in all cases. The separate frequency response region of each path is shown: the MP response occurs at the middle frequencies, while the leakage response is limited to low frequencies and the SP response is at high frequencies. Destructive interference between MP and SP transmissions is shown at 3.5 kHz in figure 7A and at 2.1 kHz in figure 10A. This interference is due to comparable transmission magnitudes and near-180° phase difference for motion above the MP resonant frequency and below the SP resonant frequency (shown in the lower panel of figure A2). Indications of interference between the MP and LP paths are shown at 0.15 kHz in figure 8B and 0.12 kHz in figure 11D. The depth of the interference dips increases with the *Q* and close resonant proximity of the two pistons.

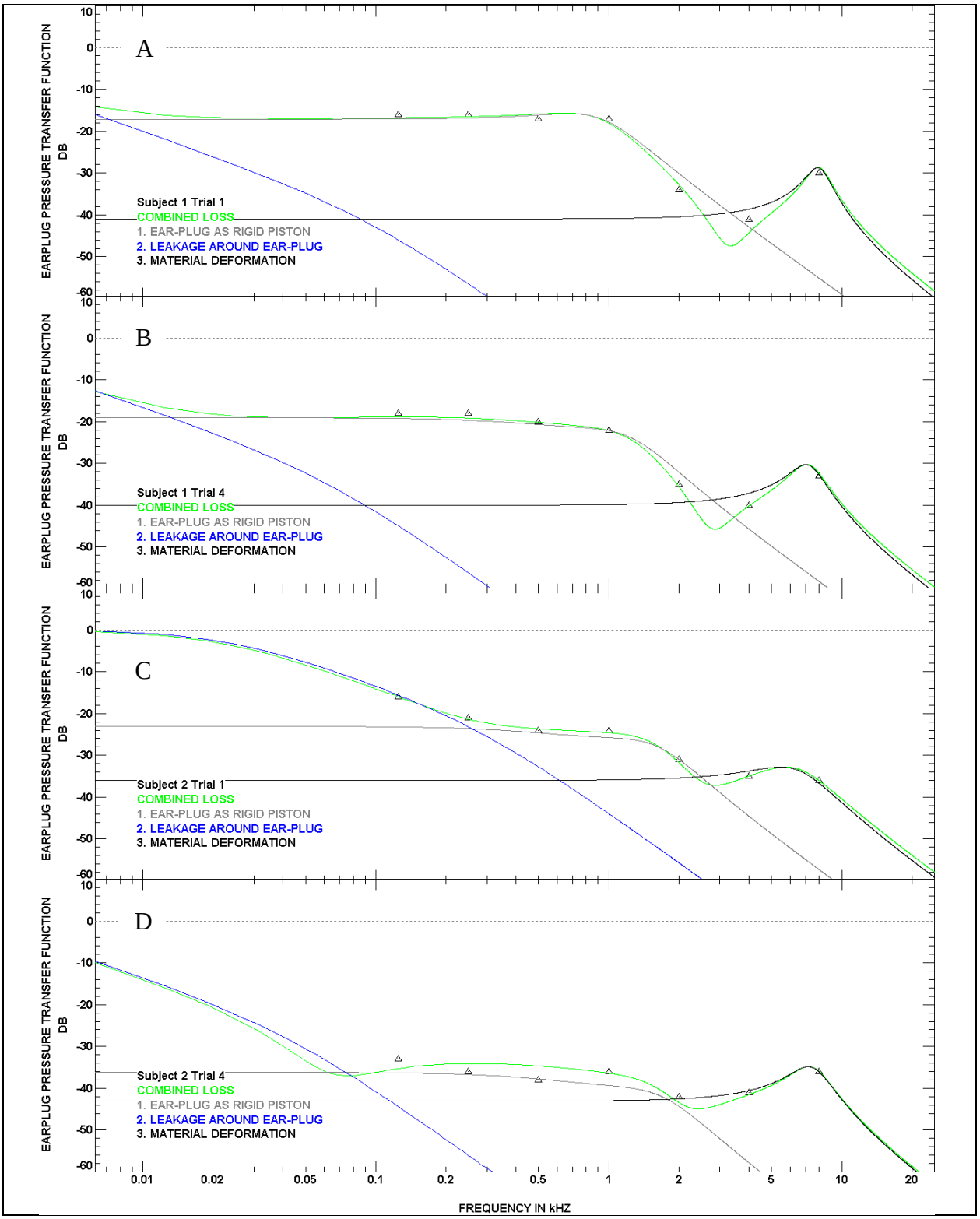

Figure 7. E.A.R. foam earplug REAT responses. Panels A and B are two trials for subject 2 with no leak and with high SP *Q* interfering with rigid piston at 3 kHz. Panel C shows a slight leak and lower SP *Q*. Panel D shows large attenuations in both rigid and SPs.

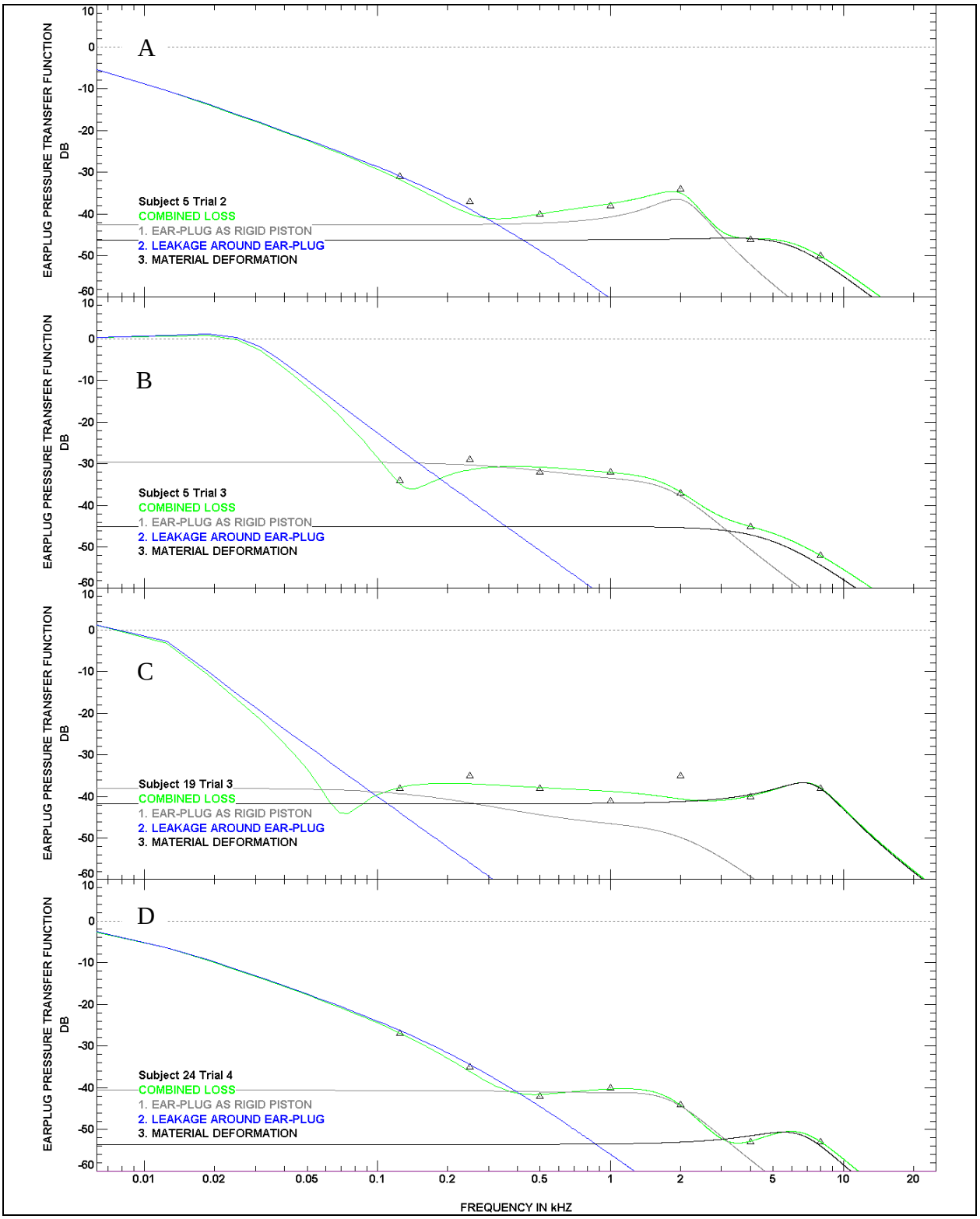

Figure 8. E.A.R. foam earplug. Panel A shows slight leak with low *Q*, rigid piston with moderately high *Q*, and SP with low *Q*. Panel B shows leak with higher *Q*, causing interference with rigid piston at 125 Hz. Panel C shows lower *Q* rigid piston with more transmission by SP. Panel D shows three transitions for all three pistons.

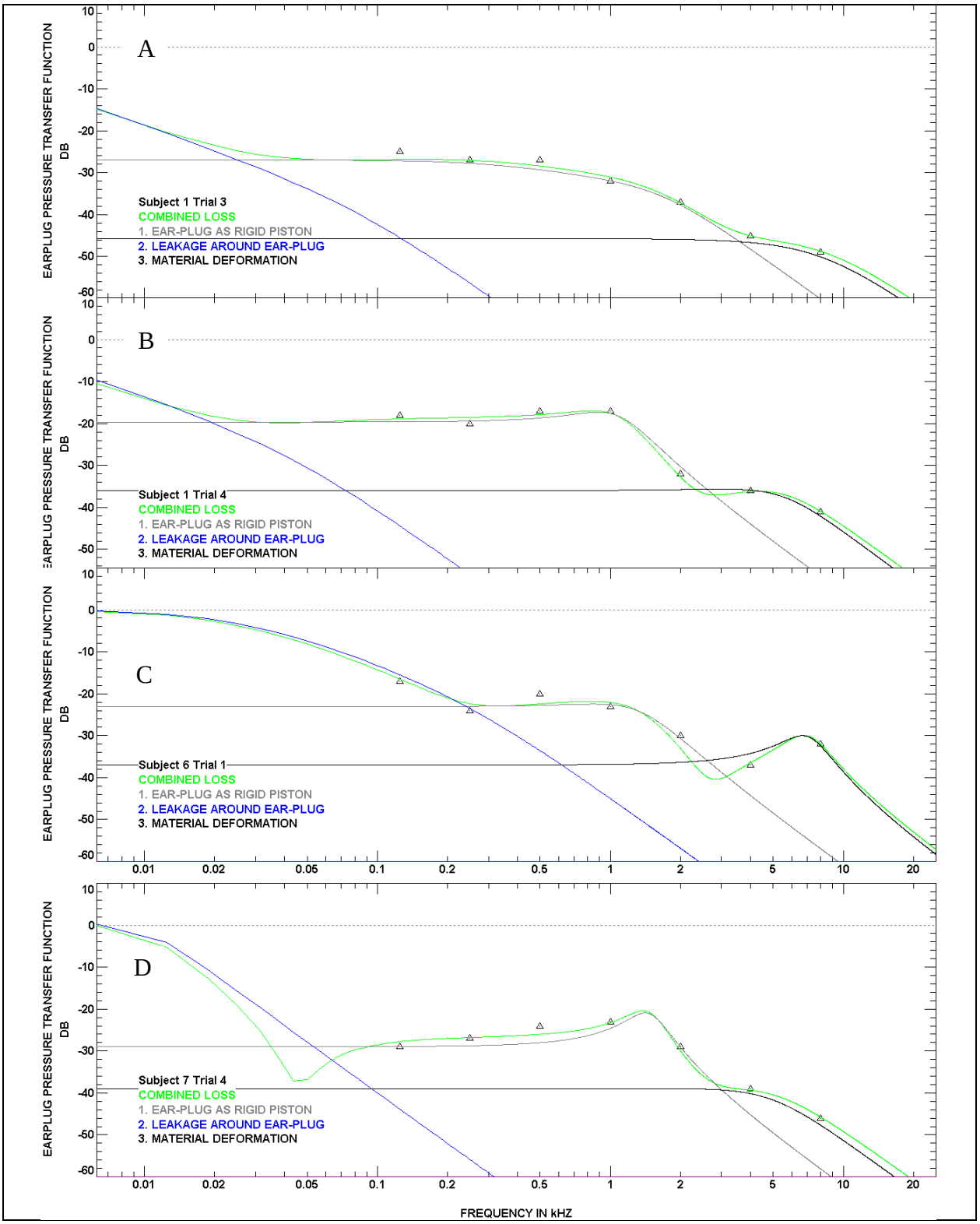

Figure 9. EP100 earplug. Panel A shows large attenuation from rigid piston with low *Q*s for this and the SP. Panel B shows higher *Q* for the rigid piston. Panel C shows a leak with interference at 2.5 kHz between rigid and SPs. Panel D shows the rigid piston with high *Q*.

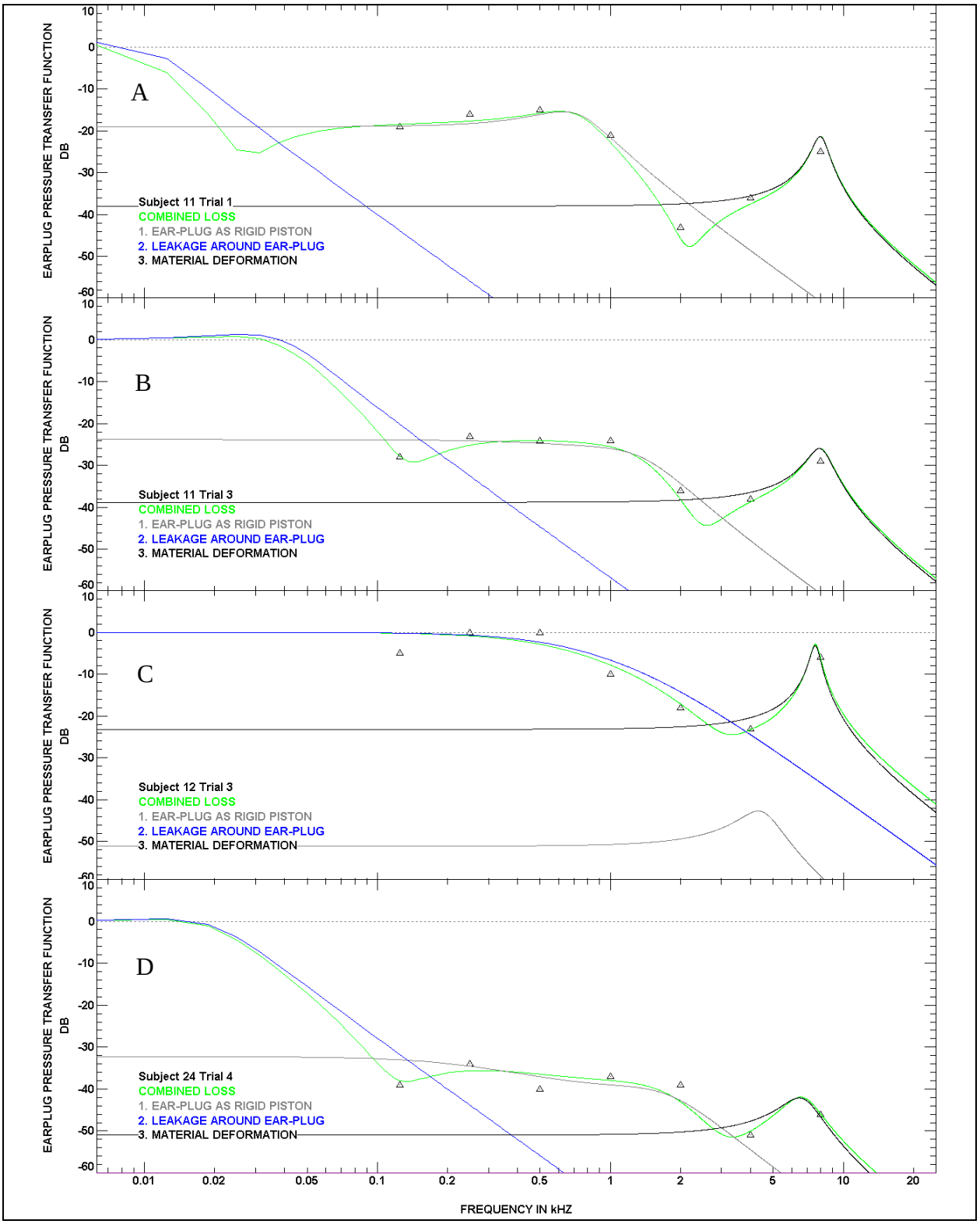

Figure 10. EP100 earplug. Panel A shows interference at 2.2 kHz between rigid piston and high *Q* SP. Panel B shows interference between rigid piston and both high *Q* leak and high *Q* SP. Panel C shows very high loss rigid piston bypassed by leak and high *Q* SP. Panel D shows interference at 125 Hz between rigid piston and high *Q* leak.

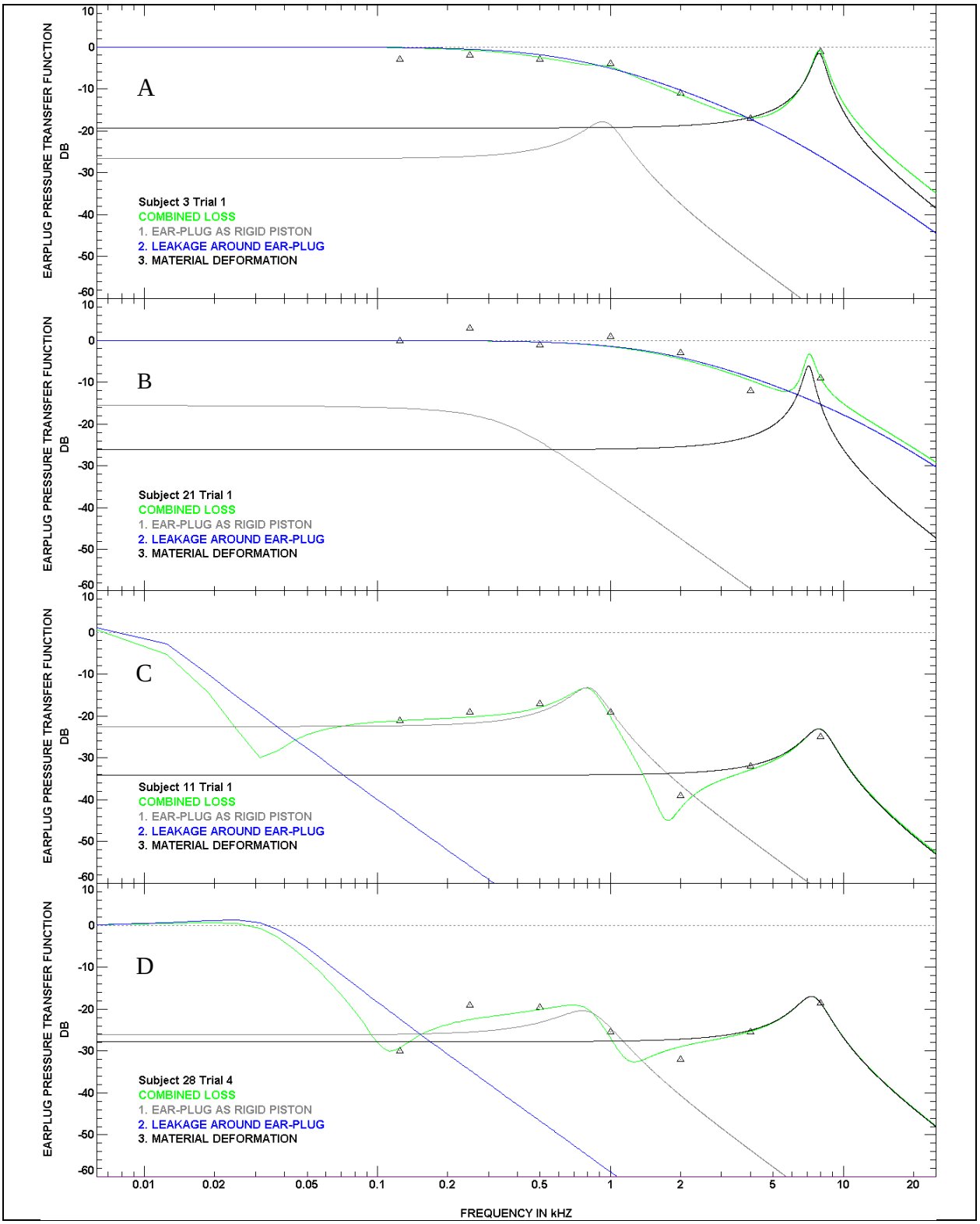

Figure 11. V-51R earplug. Panels A and B show rigid piston bypassed by leak and high *Q* SP. The leak in Panel B is greater than in A. Panel C shows strong interference at 1.7 kHz between moderately high *Q* rigid and SPs. Panel D shows interference at 110 Hz between rigid piston and high *Q* leak.

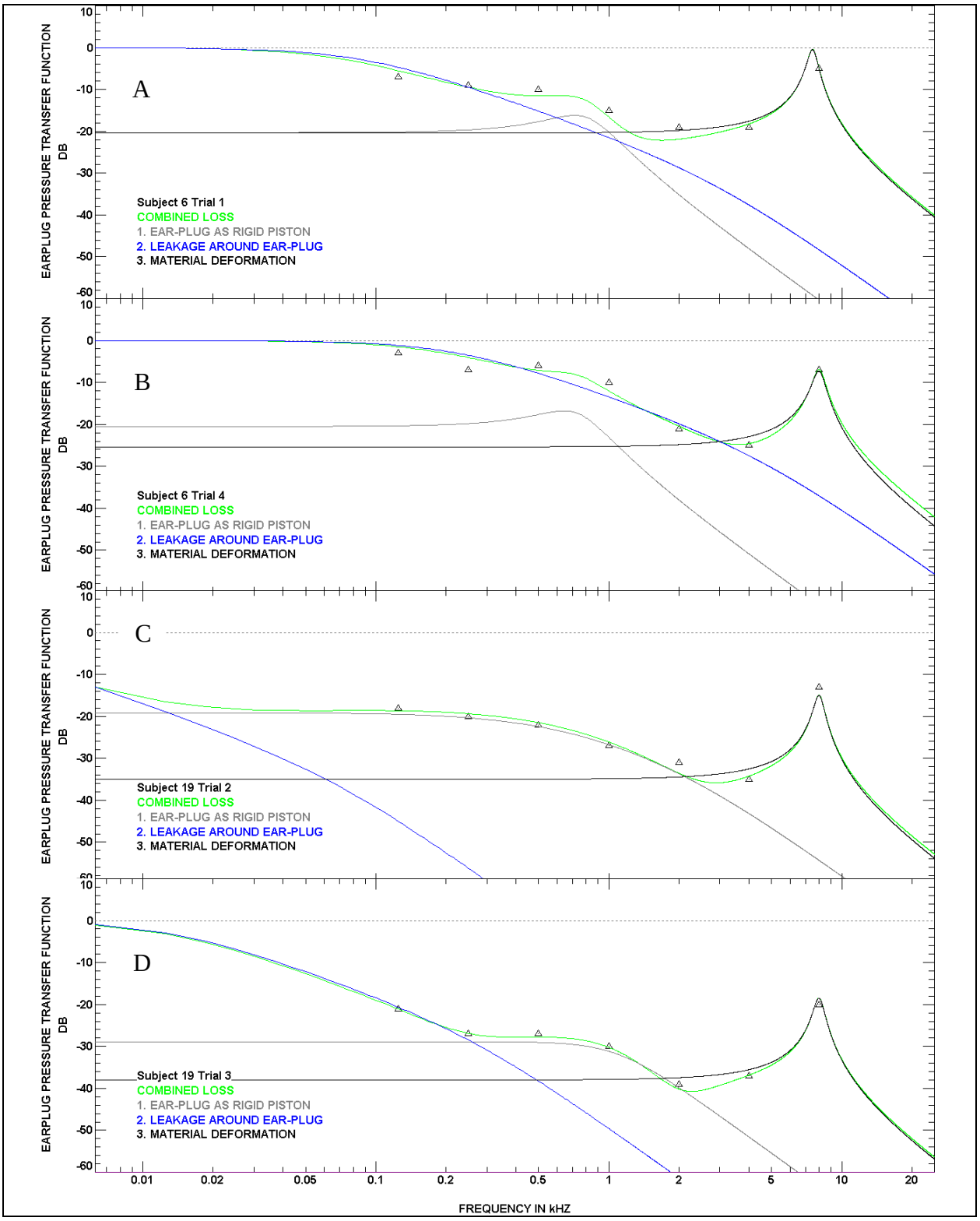

Figure 12. V-51R earplug. Panel A shows rigid piston effects between 500 and 1000 Hz with transmission mostly due to leak and SPs. Panel B shows another trial with the same subject with more leak transmission. Panel C shows rigid piston with lower *Q* and SP with high *Q*. Panel D shows slight leak and SP with high *Q*.

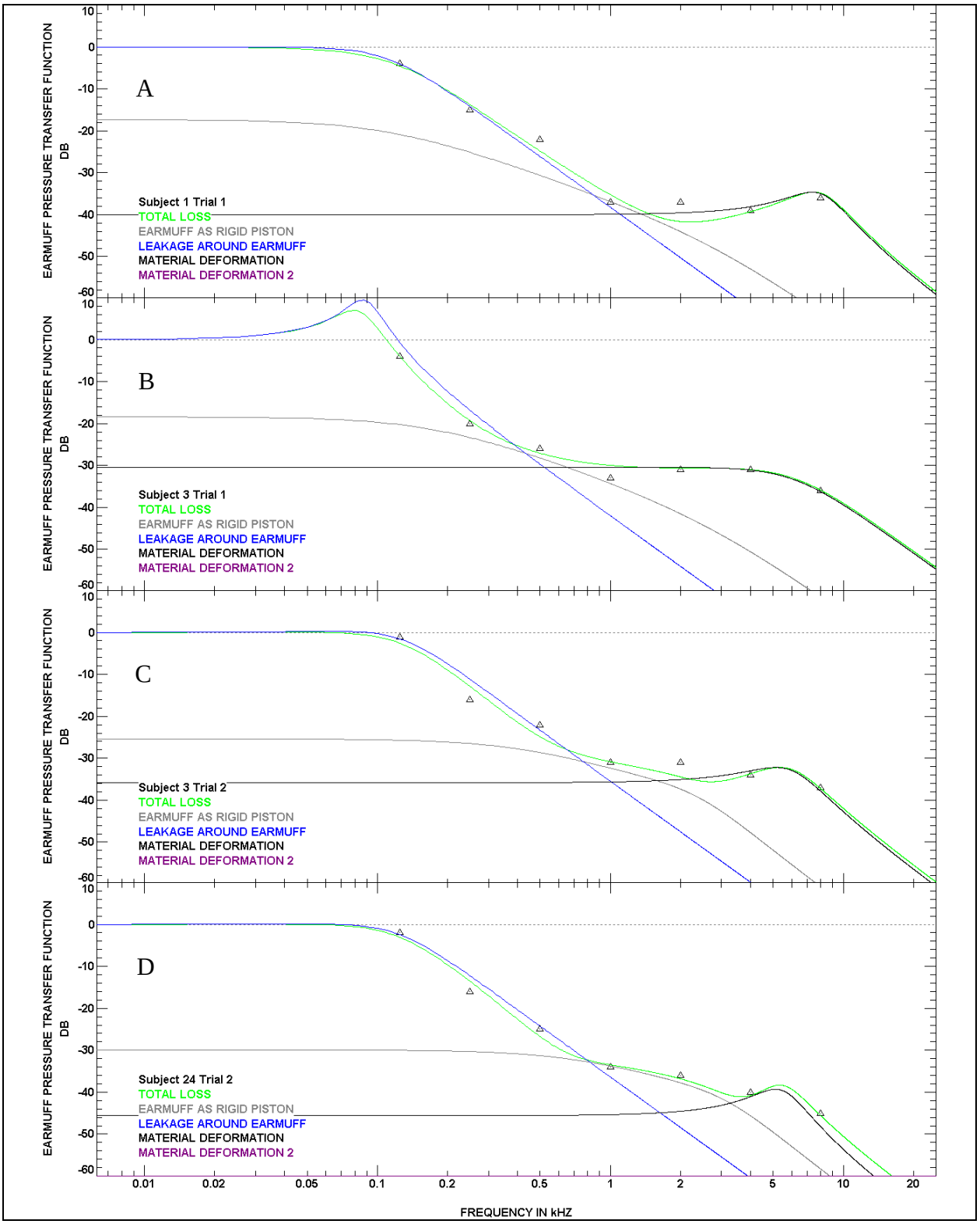

Figure 13. Bilsom UF-1 Earmuff. Panel A shows low *Q* rigid piston bypassed by moderate *Q* leak and SPs. Panel B shows high *Q* leak and moderate *Q* SPs bypassing rigid piston. Panel C shows slight rigid piston transmission between 1 and 2 kHz. Panel D shows more rigid piston transmission due to lower transmission through SP.

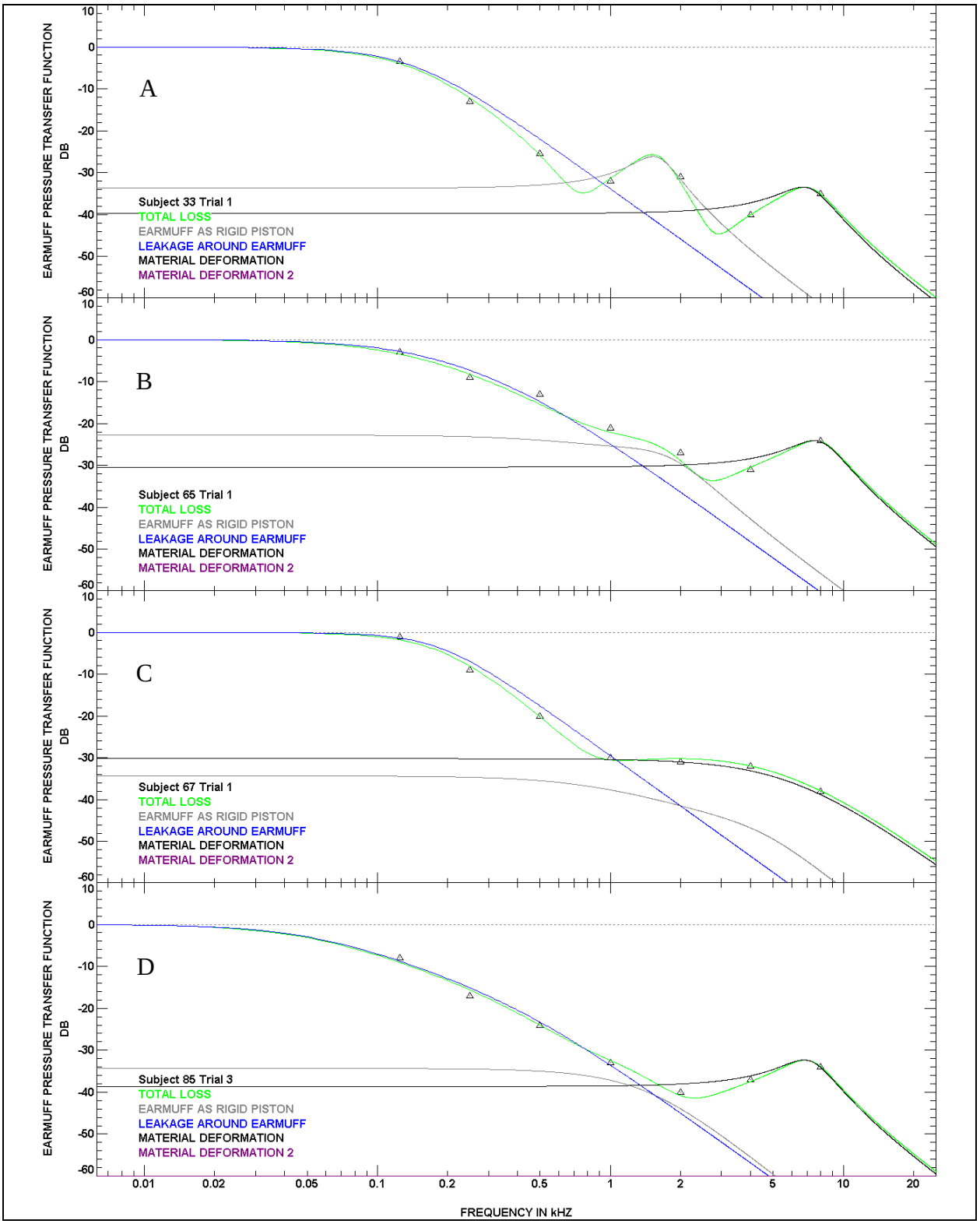

Figure 14. Bilsom UF-1 Earmuff. Panel A shows significant rigid piston transmission and interference with leak and SPs. Panel B shows less interference and transmission due to lower *Q* in both rigid piston and leak. Panels C and D show leak and SP bypassing rigid piston. D shows interference between these two paths because of higher *Q* SP.

Figure 15 shows the distributions of values for two selected simulator parameters, the OV compliance, C_V = vol/$\rho_o c^2$ (here vol = volume of the OV and $\rho_o c^2$ = acoustical compliance of air, as shown in figures 1 and 2), and the leak resistance, R_{lk} for all four data sets used in the Interlab study. In figure 15A, the foam E.A.R. earplug compliance is clustered more at the lower values, meaning the OV was smaller than for the other two earplugs. The multiple sizes of V-51R plugs give a wider distribution in compliance and hence in volume. The values vary from roughly half the mean to double the mean. Figure 15B shows C_V for the Bilsom earmuff, which is about 100 times greater than for the foam earplug. This corresponds to the OV being 100 times greater for the earmuff. Figure 15C shows the leakage resistance R_{lk} for the three earplugs with the V-51R and EP100 plugs being most probable at the lower values near 2000 units. This indicates a substantial number of leaks compared to almost none for the foam earplug with its wide range of higher values. Figure 15D shows the leak resistances fairly tightly clustered at low values for the earmuff. This is seen by the uniform LP contribution in REAT cases in figures 13 and 14.

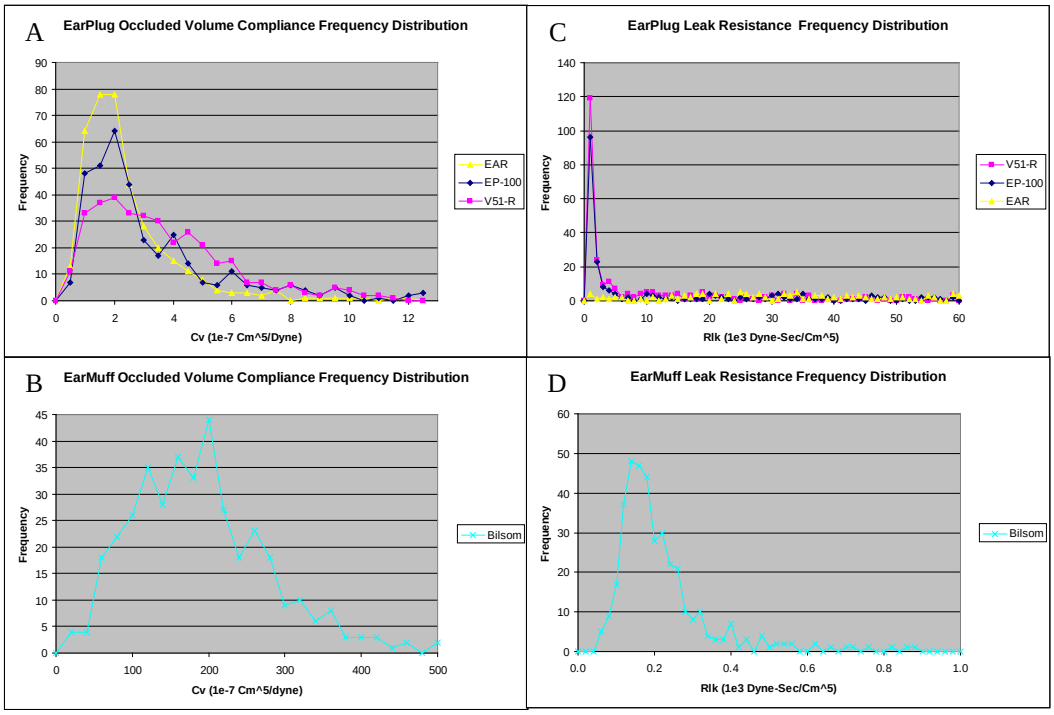

Figure 15. Statistical frequency distributions of simulator values for the 384 trials in the Interlab study. Panels A and B show the distributions of the OV compliance, C_V for the three earplugs and single earmuff. Panels C and D show the distributions of the leak resistance R_{lk} for the same protectors. The horizontal axis shows EA values in multiples 1e-7 cm^5/Dyne for the C_V plots and 1e3 Dyne-sec/cm^5 for the R_{lk} plots.

Figure 16 shows the data for the rifle waveform (figure 16C) as a stimulus applied to the model of four HPDs from Royster's study and the corresponding distributions of unwarned (figure 16A) and warned (figure 16B) auditory risk units ARU(U) and ARU(W) calculated using the AHAAH model using predicted protector waveforms. These figures show that 95% of the trials give unwarned risk values of 50 units or less for inherently well-fitting HPDs, such as the E.A.R. foam earplug and Bilsom earmuff, while the value is increased to 400 units for the poor-fitting EP100 and V51-R. Warned hazards are reduced to 10 and 90 units, respectively.

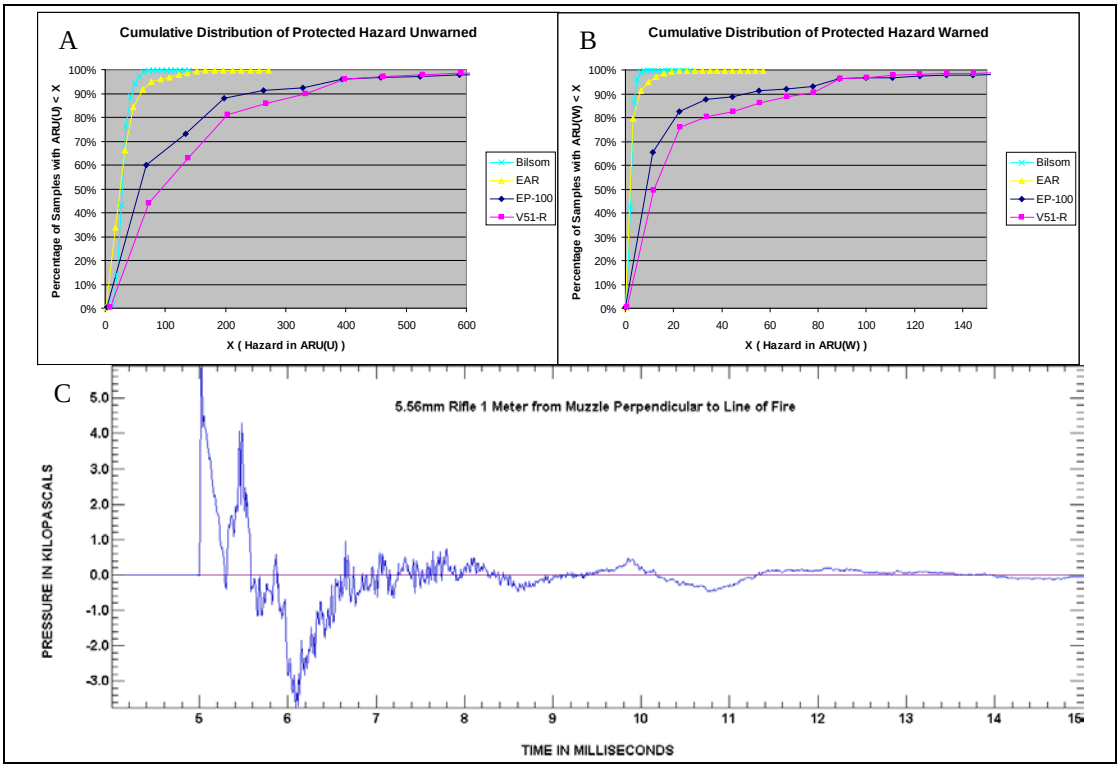

Figure 16. Cumulative distributions of protected unwarned hazard (A) and warned hazard (B) for three earplugs and single earmuff when exposed to a rifle shot shown in panel C.

The AHAAH risk units when divided into 500 give the allowed number of rounds that can be fired per day. This number can be used to select a particular HPD worn for a given stimulus.

Figure 17 shows model fits for the E.A.R. foam earplug and Combat Arms Earplug (CAE) based on REAT data provided by 3M Corporation. Figure 18 shows the model prediction for a 155-mm howitzer and ISL ATF measurements with the E.A.R. foam earplug. The upper panel shows the FF wave at the manikin (blue) and the predicted waveform (red) at the manikin eardrum. The lower panel shows the manikin measurement in blue superimposed on the same prediction in red. Figure 19 shows the prediction for an M-4 rifle and ISL manikin measurement with the CAE earplug. The upper panel shows the FF wave (blue) at the manikin and the predicted waveform (red) at the manikin eardrum. The lower panel shows the manikin measurement in blue superimposed on the same prediction in red.

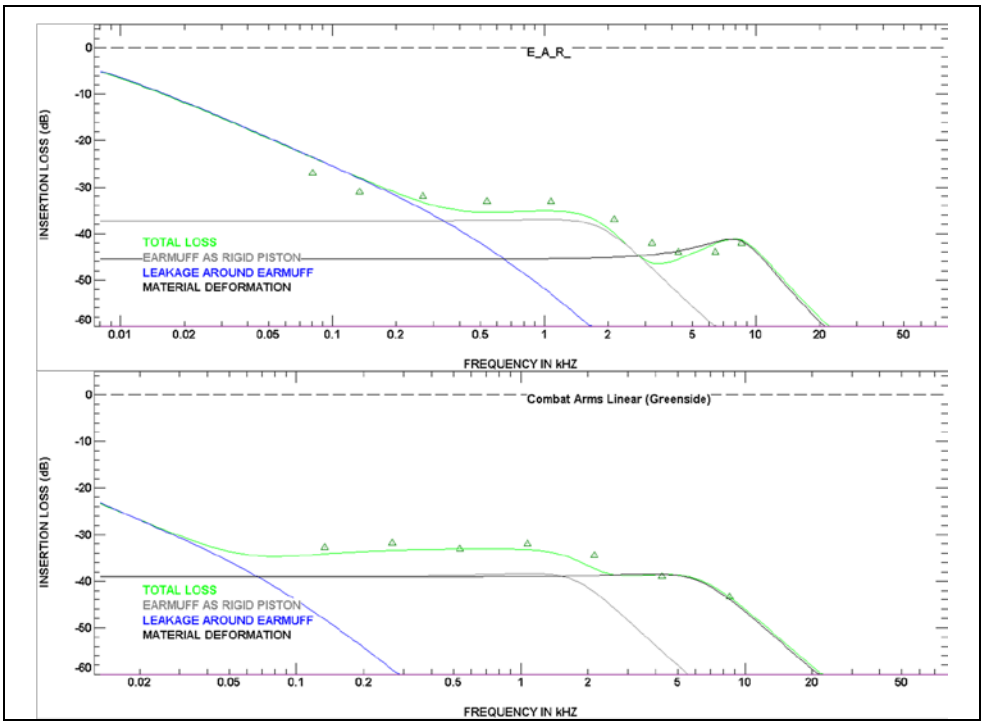

Figure 17. Manufacturer-provided REAT IL data and modeled IL data for E.A.R. foam and Combat Arms linear (greenside) earplugs.

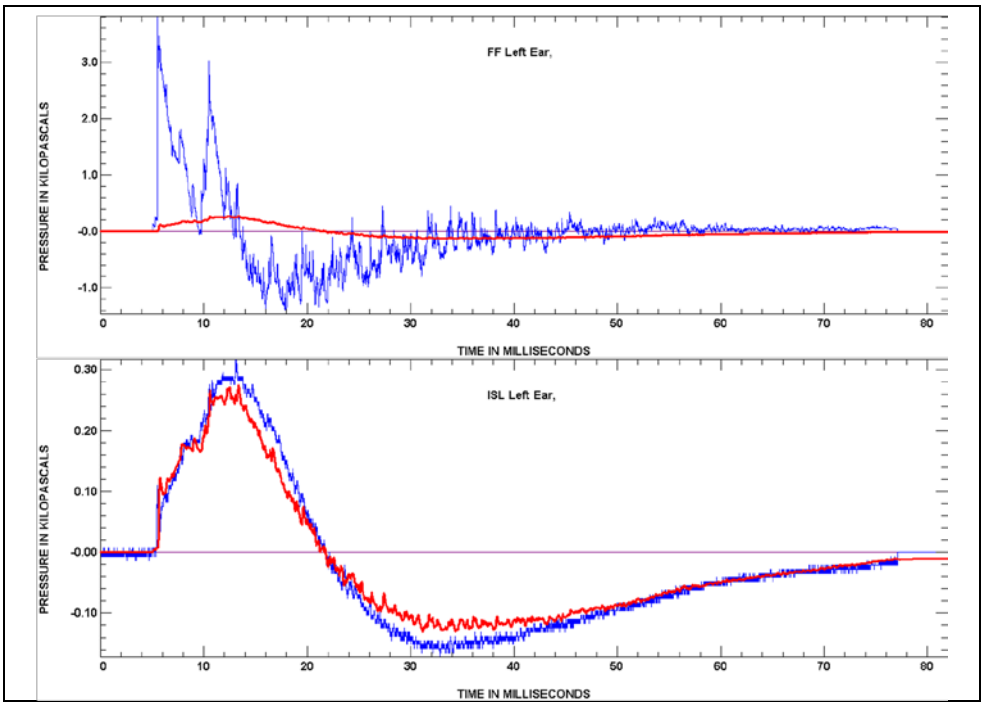

Figure 18. Results of HPD simulator applied to 155-mm howitzer at 90 ft from the ISL manikin wearing the E.A.R. foam earplug.

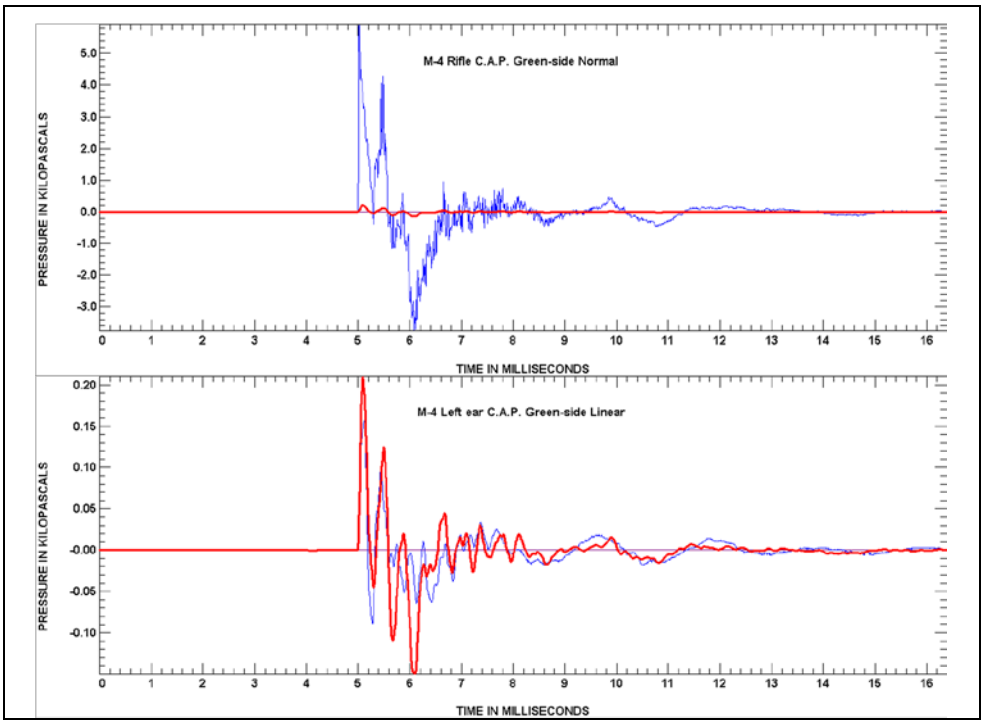

Figure 19. Results of the HPS applied to M-4 rifle at 1 m from ISL manikin wearing the linear Combat Arms earplug.

3.1 Albuquerque (ABQ) Test

The U.S. Army conducted extensive tests where volunteers were exposed to simulated weapon blasts ranging from 173- to 194-dB peak pressure levels. The earmuffs, worn under the helmet, were either intact or modified with leak-producing tubes inserted in the cushion (Patterson and Johnson, 1994). Simultaneous pressure measurements were made under the earmuffs of three subjects and in the FF. Hearing loss was assessed using temporary threshold shifts measured 2 min after the exposures. The test was named after its location in Albuquerque, NM, and is abbreviated as the ABQ test. The test site and HPDs used in the test are shown in figure 20. The HPD modified with leakage tubes is shown in the upper-right panel. Figure 21 shows REAT values provided by the experimenters and simulator fits for the intact and modified muffs. Figure 22 (upper panel) shows the simulator prediction and the measurements under the HPD for the three subjects wearing the intact muff, while figure 23 (lower panel) shows the results for the modified muff. The red lines are identical on both panels.

Figure 20. ABQ experiment showing five volunteers located 1.0 m from source in upper-left panel wearing an earmuff modified with eight tubes, shown in the upper-right panel. Other hearing protectors are shown in the lower panel, including the E.A.R. Foam and CAEs (green side is linear, yellow side is nonlinear).

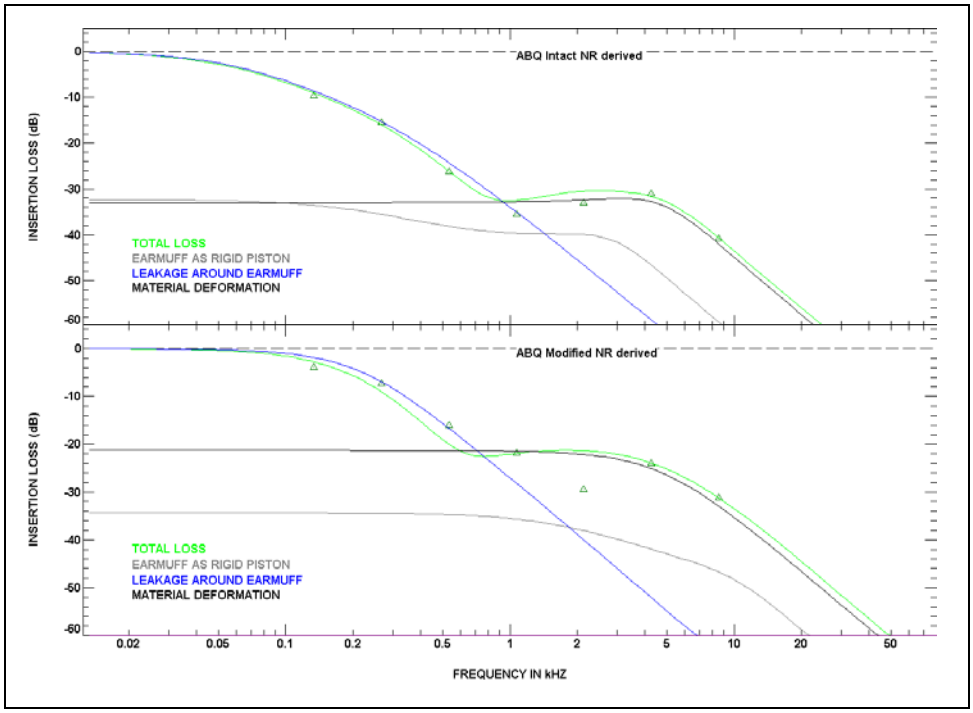

Figure 21. MIRE-derived IL measurements and fits on intact and modified ABQ earmuffs.

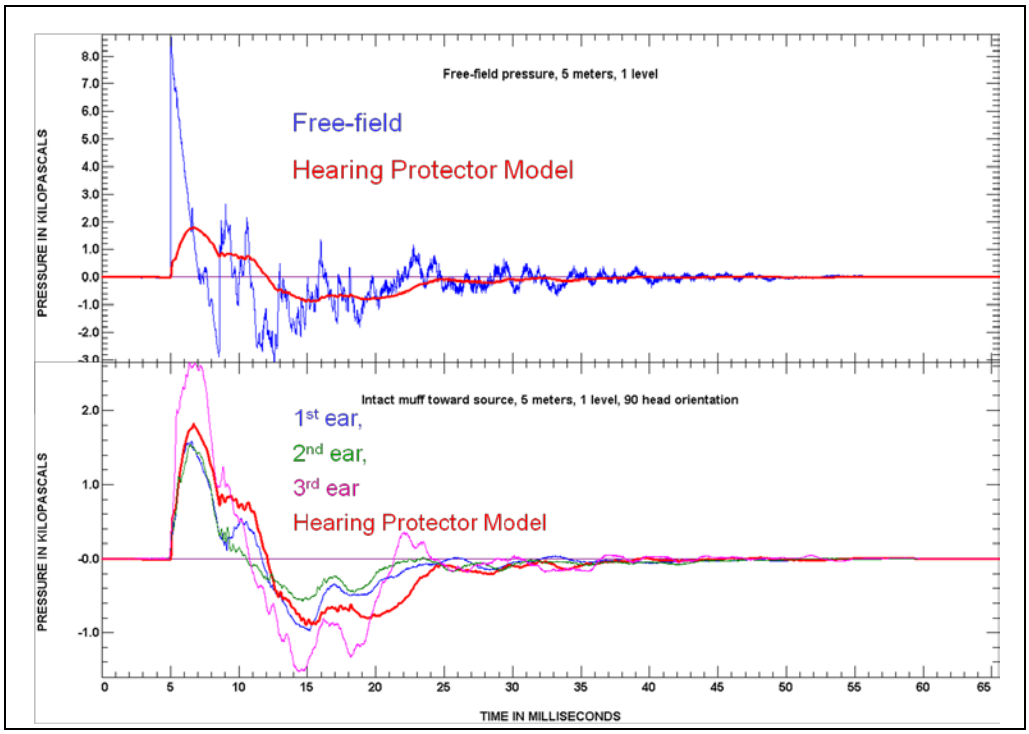

Figure 22. ABQ test results at the 5-m distance and 1-level charge strength. Upper panel shows the FF measurement in blue and the resulting HPD simulator prediction in red. Lower panel shows the HPD simulator prediction along with measurements under the intact earmuff on the ear closest to the source for the three subjects.

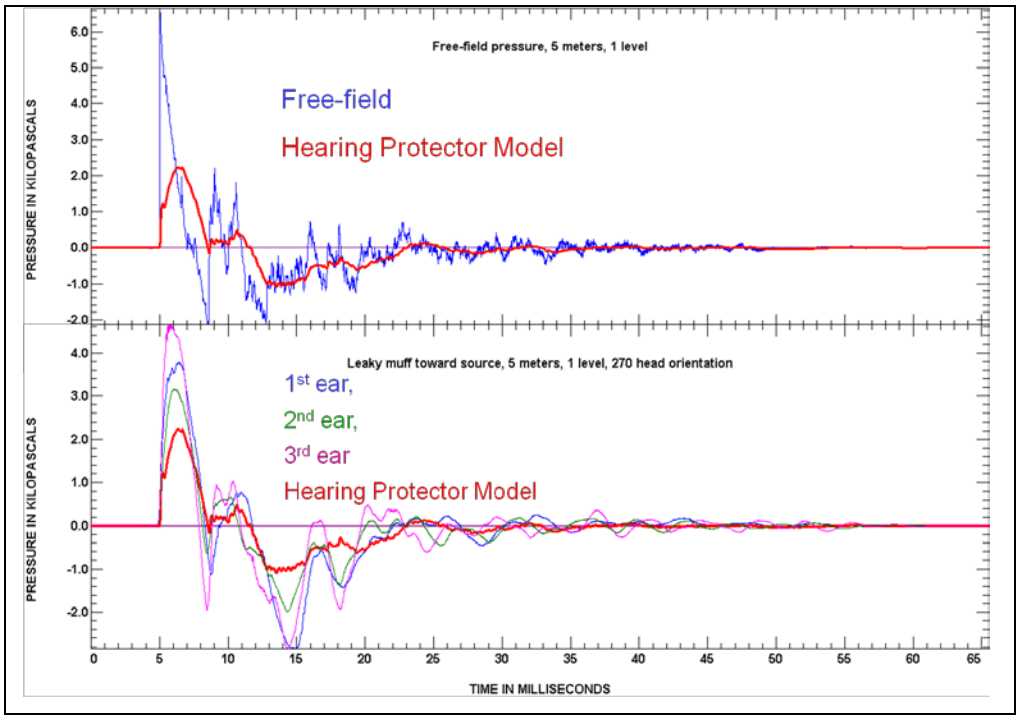

Figure 23. ABQ test results at the 5-m distance and 1-level charge strength. Upper panel shows the FF measurement in blue and the resulting HPD simulator prediction in red. Lower panel shows the HPD simulator prediction along with measurements under the modified (leaky) earmuff on the ear closest to the source for the three subjects.

The HPD simulator applies to linear HPDs with constant coefficients and adequately predicts HPD waveforms with peak pressure levels below 175 dB, which is typical of small-arms weapons. This also implies that the NR transfer function does not depend on stimulus levels and can be determined by Fourier analysis. For higher-level excitation associated with exposure near howitzers, mortars, or shoulder-fired rockets, this linear behavior may not be the case because ear cushion stiffness may increase with increased displacement, or turbulence in the orifices of the CAE may increase the viscous damping force. To study these phenomena, additional terms depending on cushion displacement or flow velocity can be added to the time domain differential equations and solved using the same numerical integration procedure used for the linear protector.

4. Conclusions

To predict the performance of earplugs and earmuffs worn during impulse noise exposure, a linear EA simulator based on protector mechanical elements and IL measurements is described herein. Three energy flow pathways associated with the protector moving as a rigid piston, leakage at the cushion-skin boundary, and multimodal vibration in the protector body are

combined in the OV to predict a pressure waveform in response to the FF impulse noise stimulus. A fitting procedure determines the individual pathway elements that control the IL in low-, medium-, and high-frequency ranges and displays the simulator response for all audible frequencies. Application of the simulator to an IL database shows statistical frequency distributions of user-fit quantities, such as leakage resistance and OV, which are useful in improving the four protector designs. As evident from calculations for a number of hearing protectors based on manufacturer supplied data, the predicted waveforms accurately match measurements made with both human and artificial ears. The simulator is expected to be a useful tool in combination with the AHAAH hearing hazard model for studying the effects of varying protector fit on the percentage of wearers protected for a given impulse noise. At present, this research can only be done with human trials with specific weapons and hearing protectors—an expensive and time-consuming process.

Future work includes adding nonlinear terms describing earmuff-cushion hardening stiffness and turbulent flow restriction through earplug orifice leaks. This work extends the low-level description determined by linear frequency analysis method to extreme levels where they would no longer be valid. Comparison with nonlinear measurements on manikin ears will be used to verify the method.

5. References

ANSI Standard S12.6-2008. *Methods for Measuring the Real-Ear Attenuation of Hearing Protectors.*

ANSI Standard S12.42-2010. *Methods for the Measurement of Insertion Loss of Hearing Protection Devices in Continuous or Impulsive Noise Using Microphone-in-Real-Ear or Acoustic Test Fixture Procedures*.

Beranek, L. L. *Acoustics*; McGraw Hill: New York, 1954**.**

Berger, E. H. Methods of Measuring the Attenuation of Hearing Protection Devices. *Journal of the Acoustical Society of America* **1986**, *79*, 1655–1687.

Kinsler, L. E.; Frey, A. R. *Fundamentals of Acoustics*, 2nd ed.; John Wiley & Sons: New York 1962.

Mehrgardt, S.; Mellert, V. Transmission Characteristics of the External Human Ear. *Journal of the Acoustical Society of America* **1977**, *61*, 1567–1576.

MIL-STD-1474D, Department of Defense Design Criteria Standard: Noise Limits, 12 February 1997.

Parmentier, G.; Dancer, A.; Buck, K.; Kronenberger, G; Beck, C. Artificial Head (ATF) for Evaluation of Hearing Protectors. *Acta Acoustica* **2000,** *86*, 847–852.

Patterson, J. H.; Johnson, D. L. Temporary Threshold Shifts Produced by High Intensity FF Impulse Noise in Humans Wearing Hearing Protection. USAARL Report. no. 94-46; U.S. Army Aeromedical Research Laboratory: Ft. Rucker, AL, 1994.

Price, G. R. Validation of the Auditory Hazard Assessment Algorithm for the Human With Impulse Noise Data. *Journal of the Acoustical Society of America* **2007**, *122*, 2786–2802.

Price, G. R.; Kalb, J. T. Insights Into Hazard From Intense Impulses From a Mathematical Model of the Ear. *Journal of the Acoustical Society of America* **1991**, *90*, 219–227.

Royster, J. D.; Berger, E. H.; Merry, C. J.; Nixon, C. W.; Franks, J. R.; Behar, A.; Casali, J. G.; Dixon-Ernst, C.; Kieper, R. W.; Mozo, B. T.; Ohlin, D.; Royster, L. H. Development of a New Standard Laboratory Protocol for Estimating the Field Attenuation of Hearing Protection Devices. Part I: Research of Working Group 11, Accredited Standards Committee S12, Noise. *Journal of the Acoustical Society of America* **1996**, *99*, 1506–1526.

Schröter, J. *Messung der Schalldämmung von Gehörschützern mit einem physikalischen Verfahren (Kunstkopfmethode) (Assessment of Hearing Protector Attenuation by a Physical Method [Dummy-Head Measurement])*, Wirtschaftsverlag NW, Bremerhaven, Fed. Rep. of Germany, **1983**.

Schröter, J.; Pösselt, C. The Use of Acoustical Test Fixtures for the Measurement of Hearing Protector Attenuation. Part II: Modeling the External Ear, Simulating Bone Conduction, and Comparing Test Fixture and Real-Ear Data. *Journal of the Acoustical Society of America* **1986**, *80*, 505–527.

Shaw, E. A. G.; Thiessen, G. J. Improved Cushion for Ear Defenders. *Journal of the Acoustical Society of America* **1958**, *30*, 24–36.

Shaw, E. A. G.; Thiessen, G. J. Acoustics of Circumaural Earphones. *Journal of the Acoustical Society of America* **1962**, *34*, 1233–1246.

Shaw, E. A. G.; Vaillancourt, M. M. Transformation of Sound-Pressure Level From the Free Field to the Eardrum Presented in Numerical Form. *Journal of the Acoustical Society of America* **1985**, *78*, 1120–1123.

Wiener, F. M.; Ross, D. A. The Pressure Distribution in the Auditory Canal in a Progressive Sound Field. *Journal of the Acoustical Society of America* **1946**, *18*, 401–408.

Zwislocki, J. Ear Protectors. In *Handbook of Noise Control*; Harris, C. M., Ed.; McGraw-Hill: New York, 1957; pp 1–27; Chapter 8.

Appendix A. Basic Electroacoustical Elements and Calculations

A.1 Ideal Piston

An ideal piston is a mass separating two regions that moves by fluid pressure or mechanical force and is supported by viscous and elastic restoring forces. It is usually rigid, but it may be an air plug where all the particles move in phase, as in or near air ducts. It also seals the regions on each side so there is no particle flow through the piston material or the supporting elements. The piston shape may be a cylindrical plug, as in an earplug, or a thin hemispherical shell, as in an earmuff. The support may be shearing material layers on the periphery of the earplug and in the inner wall of the ear canal. For the earmuff, the support is a ring of compressible material in the cushion and the nearby layer of skin. Both types of pistons have a cross-sectional area, S, and contain an occluded volume, OV, with amount, V_{occ}, which is compressed by the piston as a compliance. There is no transmission through the supporting elements. Assuming the OV compliance is fixed, the piston (also called RLC) schematic, shown in figure A-1, can be characterized by three physical parameters (R_1 , L_1 , C_1) or equivalently by three frequency domain characteristics (α_2 , f_2 , Q_2). Here, α_2 is the low-frequency attenuation level determined by pressure division across the supporting and occluded compliance. The resonant frequency and quality factor are f_2 and Q_2, respectively. The attenuation level α_2 is related to the low-frequency gain factor, K_2, by $\alpha_2 = 20 \log_{10}(K_2)$ or $K_2 = 10^{(\alpha_2/20)}$.

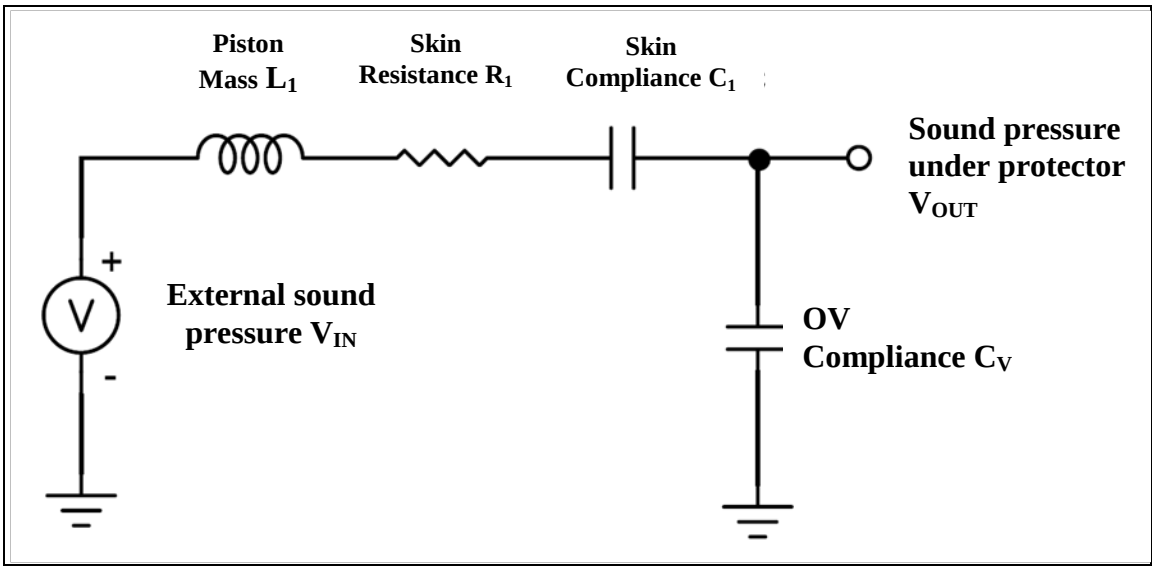

Figure A-1. Schematic diagram of the rigid-sealed main piston with mass L_1 supported by the skin compliance C_1 and resistance R_1, and enclosing the OV with compliance C_V. Similar schematics can be drawn for the leakage pistons and secondary pistons with the appropriate electroacoustic circuit elements shown in figure 1.

This circuit can be solved to give the following equation for the current, *i*.

$\frac{d\,i}{d\,t} = \frac{1}{L_1}\left(v - i\,R_1 - q\left(\frac{1}{C_1} + \frac{1}{C_V}\right)\right) = F\left(v, q, i\right)$, where the input voltage $v_{in} = v_{in}(t)$ is a function of time *t*.

The output voltage is $v_{out} = \frac{q}{C_V}$.

This is a second-order differential equation in q of the form $i' = F\left(t, q, i\right)$ and $q' = i$ with initial conditions $q_0 = 0,\ i_0 = 0$. The Runge-Kutta method of numerical integration[1] gives updated values of $\left(t_{n+1}, q_{n+1}, i_{n+1}\right)$ in terms of $\left(t_n, q_n, i_n\right)$.

$$t_{n+1} = t_n + h$$

$$q_{n+1} = q_n + h\left(\mathrm{i}_n + \frac{1}{6}\left(k_1 + k_2 + k_3\right)\right) + O\left(h^5\right)$$

$$i_{n+1} = i_n + \frac{1}{6}\left(k_1 + 2k_2 + 2k_3 + k_4\right)$$

$$k_1 = h\,F\left(t_n, q_n, i_n\right)$$

$$k_2 = h\,F\left(t_n + \frac{1}{2}h, q_n + \frac{h}{2}i_n + \frac{h}{8}k_1, i_n + \frac{k_1}{2}\right)$$

$$k_3 = h\,F\left(t_n + \frac{1}{2}h, q_n + \frac{h}{2}i_n + \frac{h}{8}k_1, i_n + \frac{k_2}{2}\right)$$

$$k_4 = h\,F\left(t_n + h, \quad q_n + h\,i_n + \frac{h}{2}k_3, i_n + k_3\right)$$

This method employs an autoadaptive step size algorithm[2] in which two integrations are carried out over the same time interval, Δt, the first with a step size of h (number of steps n) and the second with a step size of h/2 (number of steps 2n), giving results $q^{(1)}$ and $q^{(2)}$. The error estimate for the correct answer *q* is given as $q - q^{(2)} = \frac{q^{(2)} - q^{(1)}}{15}$, and if the absolute value of this is not less than an assumed error tolerance of 0.1%, then the step size is halved and the calculation is performed again. After the tolerance is met, the next time interval is calculated. If the error tolerance is met, then the step size is lengthened by dividing the total number of steps by an empirically derived value of 2.7 and rounded to a new integer number of steps and the calculation is repeated. If the error tolerance is not met, then the number of steps is doubled, and

[1]Abramowitz, M.; Stegun, I. A. *Handbook of Mathematical Functions*: U.S. Government Printing Office: Washington, DC, 1964; p 897.

[2]Press, W. H.; Teukolsky, S. A.; Vetterling, W. T.; Flannery, B. P. *Numerical Recipes in C, The Art of Scientific Computing*, 2nd ed.; Cambridge University Press: New York, 1992; p 715.

the calculation is repeated. In this way, the number of steps over each time interval is the least number required to maintain the given error tolerance.

To calculate the model frequency domain response, the Fourier transform of this differential equation and variables gives

$$V_{in} = j2\pi f L_1 I + I R_1 + \frac{1}{j2\pi f}\left(\frac{1}{C_1}+\frac{1}{C_V}\right) I \ , \quad \text{and} \quad V_{out} = \frac{I}{j2\pi f C_V} \quad \text{giving the transfer function}$$

$$A(f) = \frac{V_{out}}{V_{in}} = \frac{K_2}{1-\left(\frac{f}{f_2}\right)^2 + j\left(\frac{f}{f_2}\right)\frac{2}{Q_2}} \quad = \quad |A(f)|\, e^{-j\theta}$$

$$|A(f)| = \frac{K_2}{\sqrt{\left(1-\left(\frac{f}{f_2}\right)^2\right)^2 + \left(\frac{f}{f_2}\right)^2\left(\frac{2}{Q_2}\right)^2}}, \qquad \theta = \tan^{-1}\frac{\left(\frac{f}{f_2}\right)\left(\frac{2}{Q_2}\right)}{1-\left(\frac{f}{f_2}\right)^2}$$

where $|A(f)|$ is the magnitude and θ is the phase, which are plotted in figure A-2.

For a given value of the OV compliance, C_V, the three circuit elements (L_1, R_1, C_1), and the three frequency response descriptors (K_2, f_2, Q_2) are related by the following transformations:

$$(L_1, R_1, C_1) \underset{C_V}{\rightarrow} (K_2, f_2, Q_2). \qquad\qquad (K_2, f_2, Q_2) \underset{C_V}{\rightarrow} (L_1, R_1, C_1)$$

$$C_{II} = \frac{1}{\frac{1}{C_1}+\frac{1}{C_V}}, \quad K_0 = \frac{C_1}{C_V} \qquad\qquad K_0 = \frac{1}{\frac{1}{K_2}-1}$$

$$K_2 = \frac{C_{II}}{C_V} = \frac{1}{\frac{1}{K_0}+1} \qquad\qquad C_1 = K_0 C_V, \quad C_{II} = K_2 C_V$$

$$f_2 = \frac{1}{2\pi\sqrt{L_1 C_{II}}} \qquad\qquad L_1 = \frac{1}{C_{II}(2\pi f_2)^2}$$

$$Q_2 = \frac{4\pi f_2 L_1}{R_1} \qquad\qquad R_1 = \frac{4\pi f_2 L_1}{Q_2}$$

These expressions will be useful in controlling the curve-fitting operations on the three-piston path model by constraining a range for the resonant frequency, the *Q*, and the low-frequency attenuation. These restrictions are then applied to circuit elements if they drift out of range.

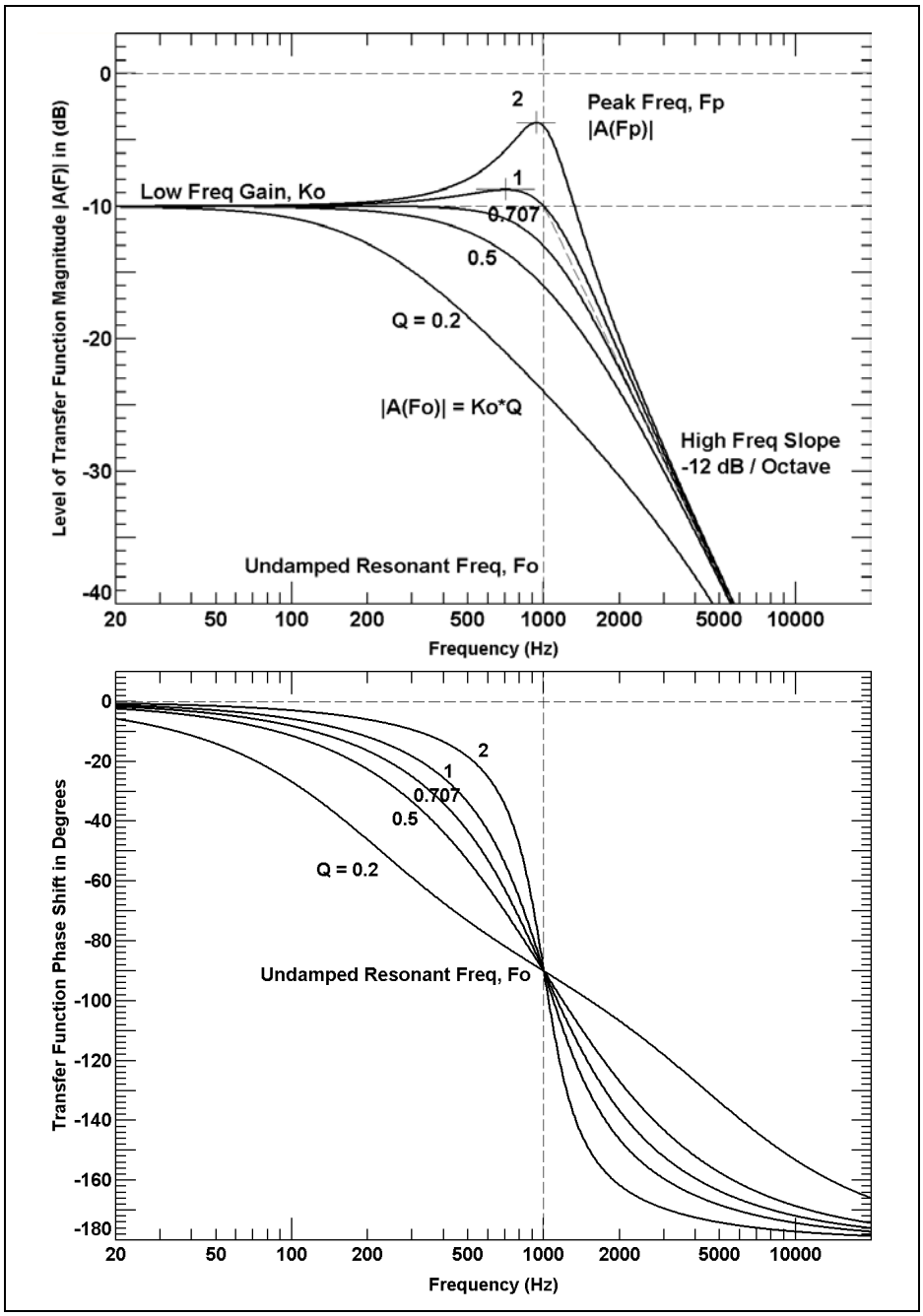

Figure A-2. Transfer function of single RLC path into the OV for given frequency f_o, quality factor Q, and low-frequency gain K_o. The upper panel plots magnitude, and the lower panel plots phase.

Each path individually forms a second-order low-pass network with the load impedance of the OV, V, given by $C_V = V/(\rho_0 c^2)$, where $\rho_0 c^2$ is the bulk compressibility of the trapped air. The three physical domain quantities R_1, L_1, and C_1 are related to the three frequency-domain quantities K_2, f_2, and Q_2. At low frequencies, the FF pressure is balanced by the combined restoring force of the compliant support structures and the compression of the OV described by

the total compliance $C_{\parallel} = \frac{1}{1/C_1 + 1/C_V}$. This forms a low-frequency loss factor given by the ratio of compliances $K_2 = \frac{C_1}{C_V}$. The piston mass resonates at an angular frequency $f_2 = 1/2\pi\sqrt{C_{\parallel} L_1}$ with a quality factor $Q_2 = \frac{2\pi f_2 L_1}{R_1}$. The *Q*-factor is defined as 2π times the total energy of a resonator divided by the amount of energy lost or gained in an oscillation cycle. *Q* is also equal to the resonant frequency *f* divided by the bandwith Δf, which is the range of frequencies for which the resonator energy is at least half of its peak value. The upper panel of figure A-2 allows the value of *Q* to be estimated from measurements of the single transmission path transfer function. The relationship between Q_2 and the damping ratio is $Q_2 = 1/2\delta_2$.

Commonly in hearing protection devices, the damping ratio $\delta_2 = 1$, which is called critical damping, and the Q_2 is then 1/2. In terms of the frequency ratio, $x = f/f_2 = \omega/\omega_2$, the frequency domain values can be read from a plot of the transfer function *A*(x) according to

$A(0) = K_1$, $A(1) = K_1 Q_2$, $A(x_P) = \frac{K_1 Q_2}{\sqrt{1 - \frac{1}{4Q_2^2}}}$, where $x_P = \sqrt{1 - \frac{1}{2Q_2^2}}$ is the peak frequency,

$A(\sqrt{2}) = \frac{K_1}{\sqrt{1 + \frac{2}{Q_2^2}}}$, $A(x) \xrightarrow[x \to \infty]{} \frac{K_1}{x^2}$, response falls off at 12 dB/octave above $x = 1$.

In the maximally flat case, $x_0 = 0$, $\delta_2 = 0.707$, $Q_2 = 0.707$, $A(x_0) = K_1$, and $A(1) = 0.707 K_1$.

In the critically damped case, $\delta_2 = 1$, $Q_2 = 0.5$, and $A(1) = 0.5 K_1$.

In the leak path, $C_3 \to \infty$ and $K_1 \to 1$, $A(1) = Q_2$.

In figure A-2, the peak labeled as 1 is derived from $Q_1 = 1$, giving $x_P = 0.707$ and $f_P = 707$ Hz. The loss at the peak frequency is $A(x_P) = 1.15\ K_1$ and the level is 1.25 dB – 10 dB = –8.75 dB.

The peak labeled as 2 is derived from $Q_2 = 2$, giving $x_P = 0.945$ and $f_P = 945$ Hz. The loss at the peak frequency is $A(x_P) = 2.07\ K_1$, and the level is 6.3 dB – 10 dB = –3.7 dB.

Note that the peak frequency approaches the resonant frequency as *Q* increases above these values. The peak value $A(x_P) = Q_2\ K_1$.

All transmission values are given in terms of K_1 and all frequencies are given in terms of f_1. The phase shifts are all 90° at resonance regardless of the *Q*. However, the rate of phase increases from 0° below resonance to 180° above resonance. This causes destructive interference between the flow velocities of the three pistons in the frequency region between their resonant frequencies.

A.2 Three-Piston Path Model and Calculations

The circuit for the earmuff along with volume velocity flows, *i*, and pressure drops, *v*, is shown in figure A-3.

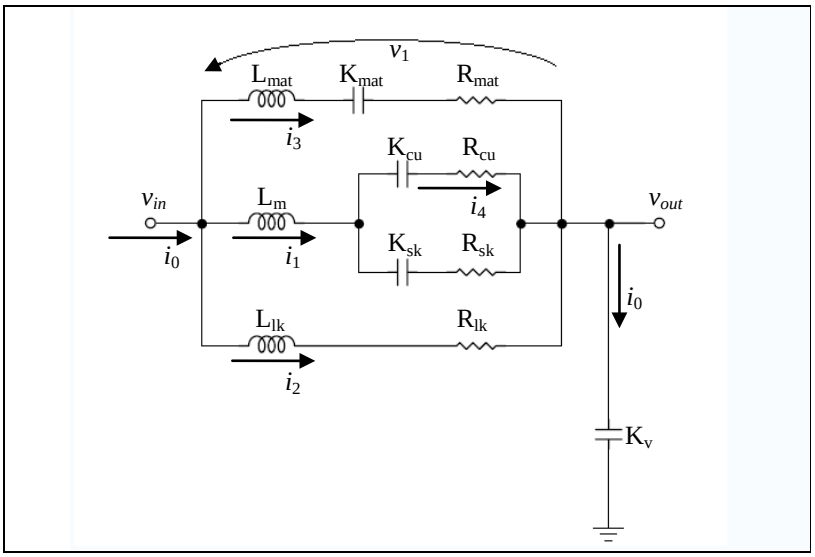

Figure A-3. Schematic diagram of the three-piston hearing protector model.

Using the expressions for the circuit elements in figure A-3, we have the following electronic network equations:

$$
\begin{aligned}
i_0 &= i_1 + i_2 + i_3 \\
v_{out} &= K_v\left(q_1 + q_2 + q_3\right) \\
v_1 &= v_{in} - v_{out} \\
\frac{di_1}{dt} &= \left(v_1 - R_{cu} i_4 - K_{cu} q_4\right) / L_m \\
\frac{di_2}{dt} &= \left(v_1 - R_{lk} i_2\right) / L_{lk} \\
\frac{di_3}{dt} &= \left(v_1 - R_{mat} i_3 - K_{mat} q_3\right) / L_{mat} \\
\frac{di_4}{dt} &= \frac{\left(R_{sk}\dfrac{di_1}{dt} + K_{sk} i_1 - \left(K_{cu} + K_{sk}\right) i_4\right)}{\left(R_{cu} + R_{sk}\right)}
\end{aligned}
$$

Integrating these equations in the same way as the basic piston gives the total volume velocity flowing into the OV, creating the pressure under the hearing protector. Likewise, the Fourier transform of these time-domain equations gives the frequency-domain equations

$$
\begin{aligned}
I_0 &= I_1 + I_2 + I_3 \\
V_{out} &= K_v I_0 / j\omega \\
V_1 &= V_{in} - V_{out} \\
V_1 &= j\omega L_m I_1 + \left(R_{cu} - jK_{cu}/\omega\right) I_4 \\
V_1 &= \left(j\omega L_{lk} + R_{lk}\right) I_2 \\
V_1 &= \left(j\omega L_{mat} + \left(R_{mat} - jK_{mat}/\omega\right)\right) I_3 \\
0 &= \left(R_{cu} - jK_{cu}/\omega\right) I_4 - \left(R_{sk} - jK_{sk}/\omega\right)\left(I_1 - I_4\right)
\end{aligned}
$$

These equations can be solved by the following method:

Let $I_4 = 1,$	velocity of ear cushion
then $I_1 = \dfrac{\left(1 + \left(R_{cu} - jK_{cu}/\omega\right)\right)}{\left(R_{sk} - jK_{sk}/\omega\right)},$	velocity of earmuff
$V_1 = j\omega L_m I_1 + \left(R_{cu} - jK_{cu}/\omega\right),$	pressure drop across hearing protector
$I_2 = V_1 / \left(R_{lk} + j\omega L_{lk}\right),$	flow velocity through leak
$I_3 = V_1 / \left(R_{mat} + j\omega L_{mat} - jK_{mat}/\omega\right),$	velocity through second piston
$V_{out} = -jK_v\left(I_1 + I_2 + I_3\right)/\omega,$	pressure under hearing protector
$V_{in} = V_{out} + V_1,$	external pressure
$A(j\omega) = \dfrac{V_{out}}{V_{in}},$	insertion loss transfer function, complex.

Appendix B. Separation of Protected Exposure Into Pure Hearing Protector Insertion Analysis Followed by Unprotected Exposure

Each block in figure B-1 represents a transfer function in the frequency domain, where frequency components are transferred from left to right. The transfer is assumed linear (at least at the low levels involved with real-ear-attenuation-at-threshold [REAT] measurements), so the magnitude and phase of the transfer depend only on the frequency.

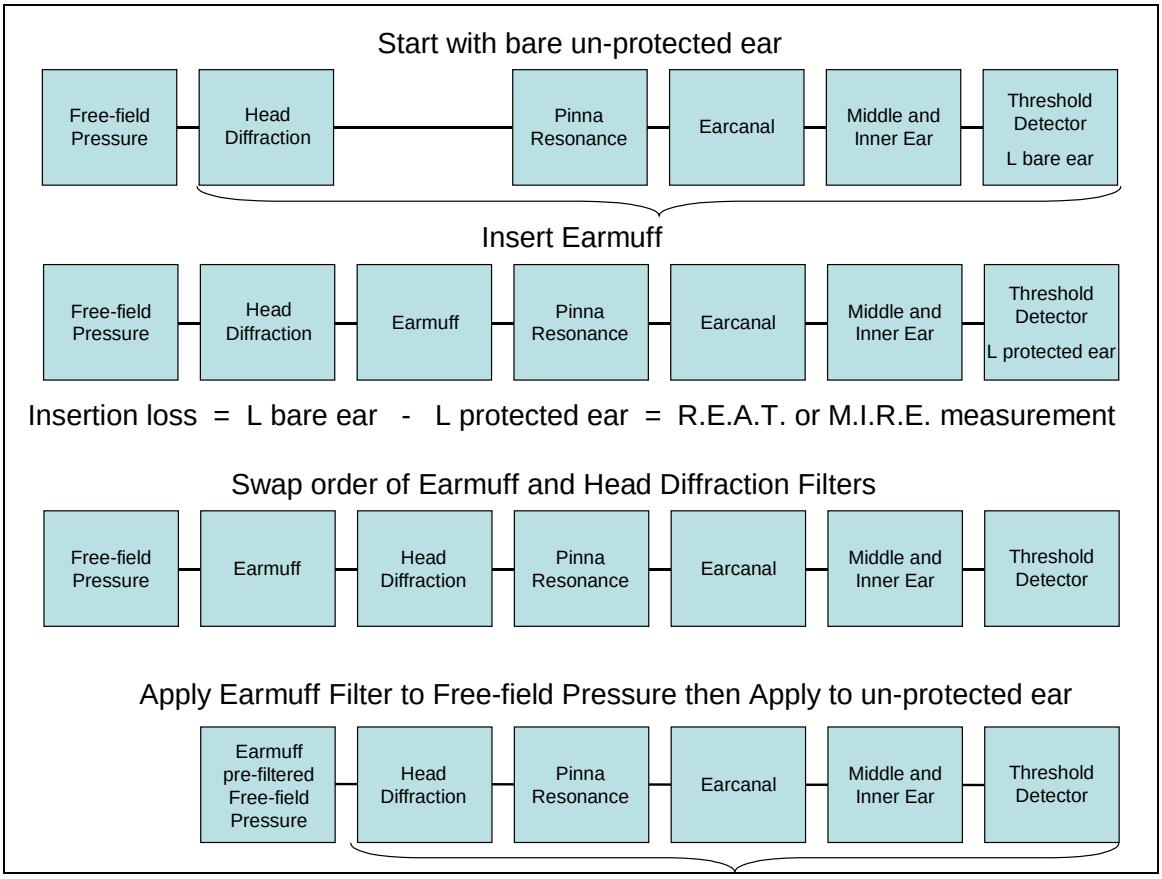

Figure B-1. Block diagram showing steps of separating protected exposure into two parts: a pure insertion loss description of the protector and a pure unprotected exposure analysis.

The free-field pressure block transfers the frequency components from near the source to a point near the head. This process may well be nonlinear since the pressure levels are high, and the blast wave loses energy to the atmosphere through heating and particle flow. Since the analysis starts at the ear, this previous history is immaterial. The Threshold Detector block transfers frequency components at the hair cells in the cochlea to a perceptual response in the REAT method denoted by the detected sound pressure level L. In the case of the microphone-in-real-ear (MIRE) method, L is the pressure level measured at an internal microphone at the eardrum location such as in the Research Institute of Saint Louis acoustic test fixture and is considered linear, provided the levels are not high enough to overload the microphone. In the case of the human ear, L is perceived and is mostly nonlinear at sound levels above 70 dB used in the REAT method due to the aural reflex in the middle ear, and the cochlear amplification due to neural

feedback to the outer hair cells. For the purposes of defining the hearing protector loss of the earmuff when REAT sound levels are below 70 dB, this detector is assumed to be linear. In the top and bottom panel, the parentheses enclose the blocks that make up the bare, unprotected ear.

Insertion of the earmuff or earplug in the second panel is most likely not an isolated event because it influences the head diffraction and pinna resonance. It is assumed that the earmuff block will overlap the two adjacent blocks. However, this is taken into account during the REAT measurement, which defines the “in-situ” loss of the hearing protector inserted onto the ear.

The electroacoustic model, assuming three loss paths, is adjusted to fit the “in-situ” loss as opposed to an “in-vitro” loss where it is mounted in a nonhuman head-like structure.

As a consequence of the linearity assumption for all the transfer functions, the order of any two can be interchanged, i.e., the loss components are commutative. Therefore interchanging the order of the earmuff and head diffraction filters reunites the components of the unprotected ear to the right of the diagram and combines the FF pressure and earmuff filter to the left. The latter two can be replaced by a prefiltered attenuated pressure waveform, which is then applied to an unprotected ear model.

This model of the hearing protector is linear and the circuit elements are considered to be low-level constant values in the time-domain linear differential equations of motion. Additional nonlinear elements can be added to the ear-cushion and skin compliance and to the leak resistance and inertia, which depend on the particle flow velocities and earmuff displacement relative to the skin. These nonlinear terms can be inserted into the equations of motion of the earmuff.

INTENTIONALLY LEFT BLANK.

Appendix C. Fitting Procedure for Insertion Loss Data

The analysis begins with the typical insertion loss (IL) frequency group {0.125, 0.25,0.5,1,2,4,8} in kilohertz by partitioning the associated loss data $\{d_1, d_2, d_3, d_4, d_5, d_6, d_7\}$ in decibels into three groups, each associated with the dominant influence of one of the three pistons. The leakage piston (LP) group is $\{d_1, d_2\}$, the main piston (MP) group is $\{d_3, d_4, d_5\}$ and the secondary piston (SP) group is $\{d_6, d_7\}$.

Initial circuit element values for earmuffs are selected from table C-1, and values for earplugs are selected from table C-2. Starting with the MP circuit elements, each is varied by 1% increments from 10% below to 10% above the starting value. The combined three-piston model values are compared to the MP group, and the sum of squared errors, E, is calculated for each increment while keeping track of the circuit element giving the lowest E. The starting element is then replaced with this new value.

Table C-1. Assumed starting values for earmuff.[1]

3.63E-09	Ccu cm^5/dyne	Acoustic area = Pi*Sqr(3.5 cm)
3.82E+04	Rcu dyne-s/cm^5	—
1.15E-06	Csk cm^5/dyne	(leak path length = 1 cm)
1.64E+04	Rsk dyne-s/cm^5	0.1 0.2 0.5 1.0 2.0 5.0 10 20 (leak diameter mm)
1.65E-01	Llk g/cm^4	2.0E1 5.0E0 8.0E-1 2.0E-1 5.0E-2 8.0E-3 2.0e-3 5.0e-4
2.31E+02	Rlk dyne-s/cm^5	7.3E5 4.6E4 1.2E3 7.3E1 4.6E0 1.2E-1 7.3e-2 1.2e0
4.05E-02	Lm g/cm^4	60-g mass
7.04E-05	Cv cm^5/dyne	7e-5 = Vcup/RhoC2: Vcup = 100 cm^3 volume
6.12E+03	Rmat dyne-s/cm^5	—
8.04E-02	Lmat g/cm^4	—
5.90E-09	Cmat cm^5/dyne	—

Table C-2. Assumed starting values for earplug.[1]

3.63E-09	Ccu cm^5/dyne	Acoustic area = Pi*Sqr (0.375 cm) Rho = 1.15e-3g/cm^3 C = 3.52e4 cm/s
3.82E+04	Rcu dyne-s/cm^5	—
1.15E-06	Csk cm^5/dyne	(leak path length = 1 cm)
1.64E+04	Rsk dyne-s/cm^5	0.1 0.2 0.5 1.0 2.0 5.0 10 20 (leak diameter mm)
2.54E+01	Llk g/cm^4	2.0E1 5.0E0 8.0E-1 2.0E-1 5.0E-2 8.0E-3 2.0e-3 5.0e-4
1.88E+04	Rlk dyne-s/cm^5	7.3E5 4.6E4 1.2E3 7.3E1 4.6E0 1.2E-1 7.3e-2 1.2e0
1.03E+01	Lm g/cm^4	2-g mass
4.65E-07	Cv cm^5/dyne	4.65e-7 = Vcup/RhoC2: Vcup = 0.66 cm^3 volume $RhoC^2$ = 1.42E6dyne/cm^2
6.12E+03	Rmat dyne-s/cm^5	—
8.04E-02	Lmat g/cm^4	—
5.90E-09	Cmat cm^5/dyne	—

[1] Schröter, J. *Messung der Schalldämmung von Gehörschützern mit einem physikalischen Verfahren (Kunstkopfmethode) (Assessment of Hearing Protector Attenuation by a Physical Method [Dummy-Head Measurement])*, Wirtschaftsverlag NW, Bremerhaven, Fed. Rep. of Germany, 1983.

This error also depends on starting errors in the other two paths, which has fixed elements in this step. After varying the MP elements sequentially, the cycle can be repeated with an increment and range either reduced or increased by a factor of 10. After each cycle is complete, the MP model is checked to see if its frequency response is still within the expected range of values for α_2, f_2, and Q_2. If any one of these values goes outside the respective range, it is replaced by that range limit. The circuit elements are then recalculated with this adjustment to prevent excessive influences from errors in the other two paths. Next, the SP circuit values are adjusted to minimize E over the SP IL group, and α_3, f_3, and Q_3 values are compared to expected limits and adjusted if necessary. Finally, the LP circuit values are adjusted to minimize the E over the LP IL group, and α_1, f_1, and Q_1 values are compared to expected limits and adjusted if necessary. If the leakage path dominates the main path, then the leakage transmission exceeds that of the MP at low to middle frequencies, and the MP is required to stay within the expected limits and not to converge to the low values because of the LP.

List of Symbols, Abbreviations, and Acronyms

ABQ	Albuquerque (test)
AHAAH	Auditory Hazard Analysis Algorithm for Humans
ANOR	allowable number of rounds
ARU	Auditory Risk Unit
ATF	acoustic test fixtures
CAE	Combat Arms Earplug
EA	electroacoustic
FF	free field
HPD	hearing protection device
HPS	hearing protector simulator
IL	insertion loss
ISL	Research Institute of Saint Louis
LP	leakage piston
MIRE	microphone-in-real-ear (method)
MP	main piston
NR	noise reduction
OV	occluded volume
REAT	real-ear-attenuation-at-threshold (method)
SP	secondary piston
TFOE	transfer function of the open ear

1 (PDF) DEFENSE TECHNICAL INFORMATION CTR DTIC OCA

2 (PDF) DIRECTOR US ARMY RESEARCH LAB RDRL CIO LL IMAL HRA MAIL & RECORDS MGMT

1 (PDF) GOVT PRINTG OFC A MALHOTRA

1 (PDF) ARMY RSCH LABORATORY – HRED RDRL HRM D T DAVIS BLDG 5400 RM C242 REDSTONE ARSENAL AL 35898-7290

1 (PDF) ARMY RSCH LABORATORY – HRED RDRL HRS EA DR V J RICE BLDG 4011 RM 217 1750 GREELEY RD FORT SAM HOUSTON TX 78234-5002

1 (PDF) ARMY RSCH LABORATORY – HRED RDRL HRM DG J RUBINSTEIN BLDG 333 PICATINNY ARSENAL NJ 07806-5000

1 (PDF) ARMY RSCH LABORATORY – HRED ARMC FIELD ELEMENT RDRL HRM CH C BURNS THIRD AVE BLDG 1467B RM 336 FORT KNOX KY 40121

1 (PDF) ARMY RSCH LABORATORY – HRED AWC FIELD ELEMENT RDRL HRM DJ D DURBIN BLDG 4506 (DCD) RM 107 FORT RUCKER AL 36362-5000

1 (PDF) ARMY RSCH LABORATORY – HRED RDRL HRM CK J REINHART 10125 KINGMAN RD BLDG 317 FORT BELVOIR VA 22060-5828

1 (PDF) ARMY RSCH LABORATORY – HRED RDRL HRM AY M BARNES 2520 HEALY AVE STE 1172 BLDG 51005 FORT HUACHUCA AZ 85613-7069

1 (PDF) ARMY RSCH LABORATORY – HRED RDRL HRM AP D UNGVARSKY POPE HALL BLDG 470 BCBL 806 HARRISON DR FORT LEAVENWORTH KS 66027-2302

1 (PDF) ARMY RSCH LABORATORY – HRED RDRL HRM AT J CHEN 12423 RESEARCH PKWY ORLANDO FL 32826-3276

1 (PDF) ARMY RSCH LABORATORY – HRED RDRL HRM AT C KORTENHAUS 12350 RESEARCH PKWY ORLANDO FL 32826-3276

1 (PDF) ARMY RSCH LABORATORY – HRED RDRL HRM CU B LUTAS-SPENCER 6501 E 11 MILE RD MS 284 BLDG 200A 2ND FL RM 2104 WARREN MI 48397-5000

1 (PDF) ARMY RSCH LABORATORY – HRED FIRES CTR OF EXCELLENCE FIELD ELEMENT RDRL HRM AF C HERNANDEZ 3040 NW AUSTIN RD RM 221 FORT SILL OK 73503-9043

1 (PDF) ARMY RSCH LABORATORY – HRED RDRL HRM AV W CULBERTSON 91012 STATION AVE FORT HOOD TX 76544-5073

1 (PDF) ARMY RSCH LABORATORY – HRED HUMAN RSRCH AND ENGRNG DIRCTRT MCOE FIELD ELEMENT RDRL HRM DW C CARSTENS 6450 WAY ST BLDG 2839 RM 310 FORT BENNING GA 31905-5400

1 (PDF) ARMY RSCH LABORATORY – HRED RDRL HRM DE A MARES 1733 PLEASONTON RD BOX 3 FORT BLISS TX 79916-6816

1 (PDF) ARMY RSCH LABORATORY – HRED HQ USASOC RDRL HRM CN R SPENCER BLDG E2929 DESERT STORM DRIVE FORT BRAGG NC 28310

8 ARMY RSCH LABORATORY – HRED
(PDF) SIMULATION & TRAINING
TECHNOLOGY CENTER
RDRL HRT COL M CLARKE
RDRL HRT I MARTINEZ
RDRL HRT T R SOTTILARE
RDRL HRT B N FINKELSTEIN
RDRL HRT G A RODRIGUEZ
RDRL HRT I J HART
RDRL HRT M C METEVIER
RDRL HRT S B PETTIT
12423 RESEARCH PARKWAY
ORLANDO FL 32826

1 ARMY G1
(PDF) DAPE MR B KNAPP
300 ARMY PENTAGON RM 2C489
WASHINGTON DC 20310-0300

ABERDEEN PROVING GROUND

22 DIR USARL
(12 PDF, RDRL HR
20 HC) L ALLENDER
P FRANASZCZUK
RDRL HRM
P SAVAGE-KNEPSHIELD
RDRL HRM AL
C PAULILLO
RDRL HRM B
J GRYNOVICKI
RDRL HRM C
L GARRETT
RDRL HRS
J LOCKETT
RDRL HRS B
M LAFIANDRA
RDRL HRS C
K MCDOWELL
RDRL HRS D
B AMREIN (20 HC)
J KALB
RDRL HRS E
D HEADLEY